Octupolar approximation for the excluded volume of axially symmetric convex bodies

Marco Piastra*
Dipartimento di Ingegneria Industriale e dell'Informazione, Università di Pavia, Via Ferrata 1, I-27100 Pavia, Italy

Epifanio G. Virga†
Dipartimento di Matematica, Università di Pavia, Via Ferrata 1, I-27100 Pavia, Italy

(Received 14 June 2013; published 25 September 2013)

We propose a simply computable formula for the excluded volume of convex, axially symmetric bodies, based on the classical Brunn-Minkoski theory for convex bodies, which is briefly outlined in an Appendix written in a modern mathematical language. This formula is applied to cones and *spherocones*, which are regularized cones; a shape-reconstruction algorithm is able to generate the region in space inaccessible to them and to compute their excluded volume, which is found to be in good agreement with our approximate analytical formula. Finally, for spherocones with an appropriately tuned amplitude, we predict the occurrence of a relative deep minimum of the excluded volume in a configuration lying between the parallel alignment (where the excluded volume is maximum) and the antiparallel alignment (where the excluded volume is minimum).

DOI: 10.1103/PhysRevE.88.032507 PACS number(s): 61.30.Cz, 47.57.J−

I. INTRODUCTION

Entropy forces are more and more recognized as the main players in the phase transitions responsible for the onset of soft matter organizations, be they of a molecular or of a supramolecular nature. We usually associate an *ordering* transition such as condensation with a process where the decrease in entropy is overcompensated by a decrease in the internal energy, so that the *free energy* of the system is reduced in the process. However, as neatly pointed out by Frenkel [1], there are systems in which the internal energy depends on the temperature but not on the density. When systems like these, at a fixed density and temperature, undergo an ordering transition, they can do so only by increasing their entropy, as the internal energy remains fixed. Systems composed only of hard-core particles, which suffer no interaction apart from the one due to the constraint of mutual impenetrability, are ideal examples of systems whose energy depends only on the temperature. Often they are simply called *hard-core* systems.

As already shown by the seminal paper of Onsager [2], long hard-core rods undergo the transition from an isotropic liquid to a liquid crystal when the density exceeds a critical value. This is an ordering transition, as the orientation of the rods' long axes is random in the low-density phase, whereas it lies along an average direction in the high-density phase. Intuitively, such a transition should lead the system into a more ordered state with less entropy; since the entropy loss cannot be compensated by an energy fall, it remains unclear whether the transition complies with the principle of minimum free energy. To appreciate that it does, one should consider that what appears as an increase in orientational order, when rods for example tend more to aligning than being randomly oriented, also amounts to an increase in mobility disorder, as more oriented rods are more at ease in gliding over one another, accessing more space than if they were orientationally disordered [1]. Thus, orientational ordering can indeed be associated with entropy increase, provided that the gain in accessible volume prevails over the loss in orientational disorder. Clearly, this is just a qualitative argument which needs to be substantiated by accurate statistical mechanics computations, but it suffices to bring attention to the volume accessible to hard particles and to the ways it is affected by their relative orientation. Maximizing the volume accessible to hard-core particles amounts to minimizing the volume they mutually exclude. Thus, the *excluded* volume between two particles is the geometric quantity that plays a central role in deciding whether otherwise counterintuitive ordering transitions can take place in hard-core systems.

Although ideal hard-core systems have long mainly existed in the realm of computer simulations, recently colloidal systems have been shown to behave very nearly as hard-core systems [1]. The last few years, in particular, have witnessed an increase in the number of theoretical studies on spontaneous aggregations of hard-core particles, from liquid-crystal assemblies to crystal and quasicrystal organization [4–6], in all of which the shape of the constituent particles matters [7]. Notwithstanding all these achievements, a clear correspondence between the particles' shape and the collective organizations they can give rise to for increasing densities is not yet available. One possible reason for that is that the excluded volume of two particles is not easily computed; fine, significant details may be concealed in the way the excluded volume depends on the particles' relative orientation, which approximate formulas are unable to reveal. This makes it desirable to devise a simple but accurate method of approximation for the excluded volume, possibly valid only in a restricted class of shapes, in which computation of the exact excluded volume for an appropriate subclass of shapes could be established with a satisfactory degree of confidence. It is the aim of this paper to provide such an approximate method for the class of axially symmetric convex bodies.

Accurate excluded volume estimates are not only needed to understand the variety of aggregation phases a system of hard-core particles can exhibit, they are also relevant to predict the behavior of proteins in solution. Most proteins have the ability to crystallize, although this seldom takes place *in vivo*, if not in

*pmarco@unipv.it
†eg.virga@unipv.it

connection with some diseases [8]. An indication of the protein propensity to crystallize has long been sought for in the dilute state. In particular, measuring (mainly by light scattering [9]) the osmotic second virial coefficient B_{22} of proteins in solution has proved an empirical effective tool to anticipate their crystallization. B_{22} is the coefficient of the quadratic correction in the mass concentration c to the osmotic pressure of the solute in a solution.[1] It has been established experimentally that protein solutions that give rise to crystallization are characterized by slightly negative values of B_{22}, while more negative values of B_{22} characterize amorphous precipitation [12,13]. These two conditions are actually believed to reflect a different character of protein-protein interactions, being of weak attraction in the former case and of stronger attraction in the latter [11]. More recently, both the interpretation of light scattering measurements of B_{22} and the significance of the above quantitative criterion to predict protein crystallization have been reexamined [14,15]. It appears that a more reliable and better justified criterion for a protein solution to be conducive to crystallization is whether the *reduced* osmotic second virial coefficient b_{22}, defined as the ratio of B_{22} to the protein mutual excluded volume, is greater or smaller than 1. In the former case, nonsteric repulsions between proteins dominate and crystallization should take place, whereas in the latter case attractive interactions dominate and crystallization should fail to take place [14,16–18]. This issue will not be further considered here; it just witnesses how the need for effective computation of the excluded volume of bodies is felt in disparate fields.

The plan of the paper is as follows. In Sec. II, we recall briefly the formal definition of excluded volume and the properties it enjoys for convex bodies, most of which build on the original work of Minkowski [19]. In Sec. III, we introduce our approximate formula for the excluded volume of axially symmetric, convex bodies, which contains the least degree of complication capable of capturing the effect of "shape polarity", which manifests itself in "tapered bodies". We show that a third-rank tensor is needed to represent appropriately such a property, thus justifying the introduction of a third-rank order tensor to describe ordered phases in assemblies of tapered, convex bodies. In Sec. IV, our approximate formula is applied to the excluded volume of circular cones. In Sec. V, our approximation is further validated by comparing its outcomes to the excluded volume computed numerically for a class of *regularized* cones through a shape-reconstruction algorithm. The regularized cones selected for this illustration are *spherocones*, that is, rounded circular cones obtained by Minkowski addition of a circular cone and a ball. This class of bodies includes both spherocylinders (which we prefer to call spherorods) and spherodisks. Finally, in Sec. VI, we collect the conclusions of our work.

Our work makes use of many known results from the geometry of convex bodies, which have enriched the mathematical literature for more than a century now. Most of these results came from classical books, some rather old; we deemed it useful for the reader to collect them in Appendix A, where they are recounted in a self-contained manner and in a unified mathematical language. Appendix B contains the technical information needed to appreciate the shape-reconstruction algorithm employed here to validate our approximate formula for the excluded volume of spherocones. It is written for the nonspecialist, and it is suggestive of possible extensions to other classes of shapes for hard-core particles.

[1]This is the pressure increment required to make the activity of the solvent in a solution of concentration c equal to that of the pure solvent at its own vapor pressure [10]. The linear dependence, to which this and higher corrections apply, is also known as the van't Hoff relation [11].

II. EXCLUDED BODY

We denote by $\mathscr{K}$ the class of all convex bodies in the three-dimensional Euclidean space $\mathscr{E}$. Appendix A, to which we refer the interested reader also for the general notation employed here, reviews the rich mathematical structure that is endowed on $\mathscr{K}$ by the *Minkowski addition*. Here we presume that the reader is already familiar with the basic concepts of convex geometry; we add only the concepts which are particularly expedient for our development.

Given two bodies, $\mathscr{B}_1,\mathscr{B}_2 \in \mathscr{K}$, the *excluded body* $\mathscr{B}_e\{\mathscr{B}_1,\mathscr{B}_2\}$ of $\mathscr{B}_2$ relative to $\mathscr{B}_1$ is the region in space that a point of $\mathscr{B}_2$ cannot access without $\mathscr{B}_1$ overlapping at least in part with $\mathscr{B}_2$. As suggested by Fig. 1, there is a clear kinematic interpretation of $\mathscr{B}_e\{\mathscr{B}_1,\mathscr{B}_2\}$, which we now recall. Conventionally, we take the centroid c_2 of $\mathscr{B}_2$ as the point describing the boundary of $\mathscr{B}_e\{\mathscr{B}_1,\mathscr{B}_2\}$ as the envelope of its trajectories in all rigid motions of $\mathscr{B}_2$ in which $\partial\mathscr{B}_2$ slides without rolling over $\partial\mathscr{B}_1$. Since $\mathscr{B}_2$ is rigid, choosing any other of its points instead of c_2 to generate $\partial\mathscr{B}_e\{\mathscr{B}_1,\mathscr{B}_2\}$ would simply amount to subjecting $\mathscr{B}_e\{\mathscr{B}_1,\mathscr{B}_2\}$ to a translation. Whenever ambiguity in unlikely to arise, to lighten our notation, we shall denote $\mathscr{B}_e\{\mathscr{B}_1,\mathscr{B}_2\}$ simply as $\mathscr{B}_e$.

Another property of the excluded body $\mathscr{B}_e\{\mathscr{B}_1,\mathscr{B}_2\}$ makes it interpretable as a special Minkowski sum. As shown in

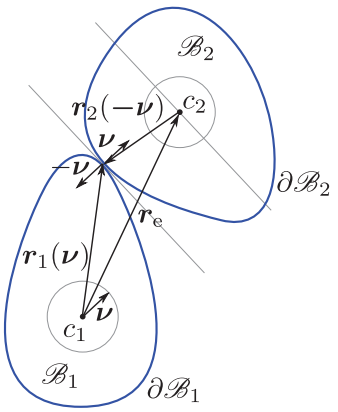

FIG. 1. (Color online) Kinematic construction of the excluded body $\mathscr{B}_e\{\mathscr{B}_1,\mathscr{B}_2\}$. Two copies of the unit sphere $\mathbb{S}^2$ are depicted around the centroids c_1 and c_2 of the bodies $\mathscr{B}_1$ and $\mathscr{B}_2$, respectively. For a given $\boldsymbol{\nu} \in \mathbb{S}^2$, $\boldsymbol{r}_1(\boldsymbol{\nu})$ translates c_1 into the point where $\partial\mathscr{B}_2$ slides without rolling over $\partial\mathscr{B}_1$, the very point where $\boldsymbol{r}_2(-\boldsymbol{\nu})$ translates c_2; $\boldsymbol{r}_1$ and $\boldsymbol{r}_2$ are the radial mappings of $\mathscr{B}_1$ and $\mathscr{B}_2$, respectively. While $\partial\mathscr{B}_2$ slides without rolling over $\partial\mathscr{B}_1$, the vector $c_2 - c_1 = \boldsymbol{r}_1(\boldsymbol{\nu}) - \boldsymbol{r}_2(-\boldsymbol{\nu})$ describes $\partial\mathscr{B}_e\{\mathscr{B}_1,\mathscr{B}_2\}$ around c_1. The two copies of the unit sphere $\mathbb{S}^2$ represent the domains of the radial mappings $\boldsymbol{r}_1$ and $\boldsymbol{r}_2$.

Appendix A [see (A5), in particular] the boundary of a convex body $\mathscr{B}$ in the special subclass $\mathscr{K}^+$ of $\mathscr{K}$ can be represented by the *radial* mapping $\boldsymbol{r}$, which establishes a one-to-one correspondence between the outer unit normal $\boldsymbol{\nu}$ to $\partial\mathscr{B}$ and the point where it is attained.[2] In our parametrization, the radial mapping delivers vectors that translate the centroid c of $\mathscr{B}$ into the points of $\partial\mathscr{B}$. For bodies $\mathscr{B}_1$ and $\mathscr{B}_2$, we denote by $\boldsymbol{r}_1$ and $\boldsymbol{r}_2$ their radial mappings, referred to the corresponding centroids c_1 and c_2 (see Fig. 1). The kinematic interpretation of the way $\partial\mathscr{B}_e\{\mathscr{B}_1,\mathscr{B}_2\}$ is generated entails that at the point of instantaneous contact between $\partial\mathscr{B}_1$ and $\partial\mathscr{B}_2$ the outer unit normals are opposite, and so the two centroids c_1 and c_2 are related through the equation

$$\boldsymbol{r}_e(\boldsymbol{\nu}) := c_2 - c_1 = \boldsymbol{r}_1(\boldsymbol{\nu}) - \boldsymbol{r}_2(-\boldsymbol{\nu}). \tag{1}$$

As $\boldsymbol{\nu}$ ranges in $\mathbb{S}^2$, $\boldsymbol{r}_e(\boldsymbol{\nu})$ describes $\partial\mathscr{B}_e$ around c_1, and we conclude that $\boldsymbol{r}_e$ is the radial mapping of $\mathscr{B}_e$. Equation (1) becomes more illuminating if, for any body in $\mathscr{K}^+$, we define the *central inverse* $\mathscr{B}^*$ as the body obtained from $\mathscr{B}$ by central inversion relative to its centroid c. Formally, if $\boldsymbol{r}$ is the radial mapping of $\mathscr{B}$, the radial mapping of $\mathscr{B}^*$ is given by

$$\boldsymbol{r}^*(\boldsymbol{\nu}) := -\boldsymbol{r}(-\boldsymbol{\nu}). \tag{2}$$

Thus (1) becomes

$$\boldsymbol{r}_e(\boldsymbol{\nu}) = \boldsymbol{r}_1(\boldsymbol{\nu}) + \boldsymbol{r}_2^*(\boldsymbol{\nu}), \tag{3}$$

which says that the excluded body $\mathscr{B}_e\{\mathscr{B}_1,\mathscr{B}_2\}$ is the Minkowski sum of $\mathscr{B}_1$ and $\mathscr{B}_2^*$ (see Appendix A for more details):

$$\mathscr{B}_e\{\mathscr{B}_1,\mathscr{B}_2\} = \mathscr{B}_1 + \mathscr{B}_2^*. \tag{4}$$

Since it readily follows from (2) that $\boldsymbol{r}^{**} = \boldsymbol{r}$, Eq. (3) also implies that $\boldsymbol{r}_e^* = \boldsymbol{r}_1^* + \boldsymbol{r}_2$, which shows that

$$\mathscr{B}_e\{\mathscr{B}_1,\mathscr{B}_2\}^* = \mathscr{B}_e\{\mathscr{B}_1^*,\mathscr{B}_2^*\} = \mathscr{B}_e\{\mathscr{B}_2,\mathscr{B}_1\}. \tag{5}$$

This equation says that, as also remarked in [20], the excluded body $\mathscr{B}_e\{\mathscr{B}_1,\mathscr{B}_2\}$ is in general *not* symmetric under the exchange of the bodies $\mathscr{B}_1$ and $\mathscr{B}_2$.[3] On the other hand, (5) implies that for two equal convex bodies $\mathscr{B}_1 = \mathscr{B}_2 = \mathscr{B}$, the excluded body $\mathscr{B}_e\{\mathscr{B},\mathscr{B}\}$ is centrally symmetric.

We imagine both bodies $\mathscr{B}_1$ and $\mathscr{B}_2$ with their centroids brought to coincide, say in the centroid c_1 of $\mathscr{B}_1$, which is then taken as the origin tacitly understood in the definition of the Minkowski addition, and which by (A48) is also the centroid of $\mathscr{B}_e$. Figure 2 illustrates the construction of $\partial\mathscr{B}_e$ based on (4): for any given $\boldsymbol{\nu} \in \mathbb{S}^2$, the centroid c_2 of $\mathscr{B}_2^*$, initially coincident with c_1, is moved in c_2^* on the boundary of $\mathscr{B}_1$ by $\boldsymbol{r}_1(\boldsymbol{\nu})$, and $c_2^* + \boldsymbol{r}_2^*(\boldsymbol{\nu})$ then designates the point on $\partial\mathscr{B}_e$ with outer normal $\boldsymbol{\nu}$.

The central inverse $\mathscr{B}^*$ of a body $\mathscr{B} \in \mathscr{K}^+$ has certain simple invariance properties which will be used in the following. First, it easily follows from (2) that the total mean curvature M defined by (A10) and represented by (A21), is invariant under central inversion. Second, since by (A11) tensors that differ by a sign have one and the same adjugate, use of (A36) and (A46b) shows that both the surface area S and the volume V are functionals invariant under central inversion. In summary,

$$M[\mathscr{B}^*] = M[\mathscr{B}], \quad S[\mathscr{B}^*] = M[\mathscr{B}], \quad V[\mathscr{B}^*] = M[\mathscr{B}]. \tag{6}$$

A body $\mathscr{B}$ for which $\boldsymbol{r}^* = \boldsymbol{r}$ is said to be *centrally symmetric*, as $\mathscr{B}^* = \mathscr{B}$.

The volume of the excluded body $\mathscr{B}_e\{\mathscr{B}_1,\mathscr{B}_2\}$ is called the *excluded volume* of the pair of bodies $\{\mathscr{B}_1,\mathscr{B}_2\}$; we shall denote it as

$$V_e\{\mathscr{B}_1,\mathscr{B}_2\} := V[\mathscr{B}_e\{\mathscr{B}_1,\mathscr{B}_2\}], \tag{7}$$

or simply as V_e, whenever explicit reference to the bodies in question can be omitted. An immediate consequence of (6) and (5) is that $V_e\{\mathscr{B}_1,\mathscr{B}_2\} = V_e\{\mathscr{B}_2,\mathscr{B}_1\}$, for all bodies $\mathscr{B}_1,\mathscr{B}_2$, and so V_e is often simply called the *mutual* excluded volume.

Equations (6) combined with (4) allow us to express the isotropic average $\langle V_e\rangle$ of the excluded volume under rotation of one body relative to the other in a rather concise form. We refer the reader to Appendix A 5 below for a formal definition of the isotropic average of a body functional. Here we are contented with borrowing Eq. (A58) to arrive at

$$\langle V_e\{\mathscr{B}_1,\mathscr{B}_2\}\rangle = V[\mathscr{B}_1] + V[\mathscr{B}_2] + \frac{1}{4\pi}(M[\mathscr{B}_1]S[\mathscr{B}_2] + M[\mathscr{B}_2]S[\mathscr{B}_1]), \tag{8}$$

where the average can be taken in either of the bodies since $V_e\{\mathscr{B}_1,\mathscr{B}_2\}$ is symmetric under their exchange.

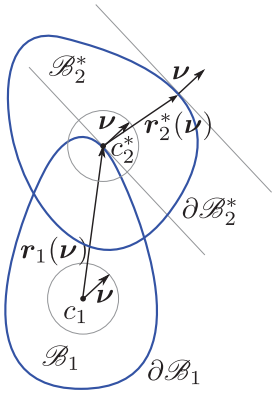

FIG. 2. (Color online) Equivalent construction of the excluded body $\mathscr{B}_e\{\mathscr{B}_1,\mathscr{B}_2\}$ as the Minkowski sum of $\mathscr{B}_1$ and $\mathscr{B}_2^*$, the central inverse body of $\mathscr{B}_2$ relative to its centroid c_2. The vector $\boldsymbol{r}_1(\boldsymbol{\nu})$ translates c_2, initially coincident with c_1, to the point c_2^* on $\partial\mathscr{B}_1$ and the vector $\boldsymbol{r}_2^*(\boldsymbol{\nu})$ further translates it on $\partial\mathscr{B}_e\{\mathscr{B}_1,\mathscr{B}_2\}$, to the point where $\boldsymbol{\nu}$ is the outer unit normal to the excluded body.

A. Symmetries

When the convex bodies $\mathscr{B}_1$ and $\mathscr{B}_2$ enjoy special symmetries, their excluded body $\mathscr{B}_e$ inherits some of their symmetries

[2] $\mathscr{K}^+$ is the class of all *strictly* convex bodies whose boundaries have *positive* principal curvatures. It is shown in Appendix A in what sense $\mathscr{K}^+$ can be regarded as *dense* in $\mathscr{K}$, which makes it sufficient for us to consider here only bodies in $\mathscr{K}^+$.

[3] We take this opportunity to correct the erroneous statement to the opposite effect in [21] (Sec. III) and [22] (Sec. II B), which however had no bearing on the development of those studies.

and special reduced formulas can be given for V_e. Here we record some of these properties, with special emphasis on those related to both central and axial symmetries, the latter being the one we are especially concerned with in this paper.

1. Central symmetry

If $\mathscr{B}_1 = \mathscr{B}_2 = \mathscr{B}$, for $\mathscr{B}$ a centrally symmetric, convex body with radial mapping $\boldsymbol{r}$, it readily follows from (3) that $\boldsymbol{r}_e = 2\boldsymbol{r}$, and so $\mathscr{B}_e\{\mathscr{B},\mathscr{B}\} = 2\mathscr{B}$ and (A52) implies that

$$V_e\{\mathscr{B},\mathscr{B}\} = 8V[\mathscr{B}]. \tag{9}$$

Similarly, if two convex bodies, $\mathscr{B}_1$ and $\mathscr{B}_2$, are centrally symmetric, then again by (3) $\boldsymbol{r}_e^* = \boldsymbol{r}_e$, which shows that $\mathscr{B}_e\{\mathscr{B}_1,\mathscr{B}_2\}$ is also centrally symmetric. By (5), then $\mathscr{B}_e\{\mathscr{B}_1,\mathscr{B}_2\} = \mathscr{B}_e\{\mathscr{B}_2,\mathscr{B}_1\}$, for any two centrally symmetric bodies $\mathscr{B}_1$ and $\mathscr{B}_2$.

2. Mirror symmetry

Let $\mathscr{B}$ be a body and let a plane be given passing through a point $o \in \mathscr{E}$ and orthogonal to the unit vector $\boldsymbol{e}_\perp$. We call the *mirror image* of $\mathscr{B}$ through $\boldsymbol{e}_\perp$ the set defined by

$$\mathscr{B}_\perp := \{p' \in \mathscr{E} \,|\, (p'-o) = \mathbf{R}_\perp(p-o),\ p \in \mathscr{B}\},$$

where $\mathbf{R}_\perp := \mathbf{I} - 2\boldsymbol{e}_\perp \otimes \boldsymbol{e}_\perp$ is the reflection through $\boldsymbol{e}_\perp$. It is easily seen that $\mathbf{R}_\perp$ is both symmetric and orthogonal and that it satisfies both $(\mathbf{R}_\perp)^2 = \mathbf{I}$ and $\det \mathbf{R}_\perp = -1$. For a body $\mathscr{B} \in \mathscr{K}^+$ with radial mapping $\boldsymbol{r}$, its mirror image is represented by the radial mapping

$$\boldsymbol{r}_\perp(\boldsymbol{v}) := \mathbf{R}_\perp \boldsymbol{r}(\mathbf{R}_\perp \boldsymbol{v}). \tag{10}$$

It readily follows from (2) and (10) that

$$(\boldsymbol{r}^*)_\perp = (\boldsymbol{r}_\perp)^*. \tag{11}$$

A body is said to be *mirror symmetric* through $\boldsymbol{e}_\perp$ if $\mathscr{B}_\perp = \mathscr{B}$. It is an immediate consequence of (A47) that a mirror symmetric body has its centroid on the plane of mirror symmetry. Suppose that a body $\mathscr{B} \in \mathscr{K}^+$ is mirror symmetric through $\boldsymbol{e}_\perp$. By (11), its radial mapping $\boldsymbol{r}$ satisfies $\boldsymbol{r}_\perp = \boldsymbol{r}$, which together with (10) also implies that $\boldsymbol{r}_\perp^* = \boldsymbol{r}^*$. It then follows easily from (3) that if two bodies $\mathscr{B}_1,\mathscr{B}_2 \in \mathscr{K}^+$ have one and the same plane of mirror symmetry so also does the excluded body $\mathscr{B}_e\{\mathscr{B}_1,\mathscr{B}_2\}$.

3. Axial symmetry

Let $\boldsymbol{e}$ be a unit vector. We denote by $\mathsf{SO}(2)$ the one-parameter group of rotations about $\boldsymbol{e}$. An explicit representation of this group is provided by the following formula:

$$\mathbf{Q}_\varphi = \mathbf{I} + \sin\varphi \mathbf{W}_e + (1-\cos\varphi)\mathbf{W}_e^2, \tag{12}$$

where $\mathbf{W}_e$ is the skew symmetric tensor with axis $\boldsymbol{e}$ and $\varphi \in [0,2\pi]$ can be interpreted as a rotation angle. A direct computation shows that $\mathbf{W}_e^2 = -(\mathbf{I} - \boldsymbol{e}\otimes\boldsymbol{e})$, which together with (12) allows one to write the reflection $\mathbf{R}_e$ through $\boldsymbol{e}$ as

$$\mathbf{R}_e = -\mathbf{I} - 2\mathbf{W}_e^2 = -\mathbf{Q}_\pi. \tag{13}$$

We shall denote by $\mathbf{Q}_\varphi\{\mathscr{B}\}$ the body $\mathscr{B}$ *rotated* by the angle φ around $\boldsymbol{e}$.[4] A body $\mathscr{B}$ is said to be axially symmetric around $\boldsymbol{e}$ if $\mathbf{Q}_\varphi\{\mathscr{B}\} = \mathscr{B}$ for all $\varphi \in [0,2\pi]$. If $\mathscr{B} \in \mathscr{K}^+$, the radial mapping $\boldsymbol{r}_\varphi$ of $\mathbf{Q}_\varphi\{\mathscr{B}\}$ is related to the radial mapping $\boldsymbol{r}$ of $\mathscr{B}$ through the equation

$$\boldsymbol{r}_\varphi(\boldsymbol{v}) = \mathbf{Q}_\varphi \boldsymbol{r}\big(\mathbf{Q}_\varphi^{\mathsf{T}}\boldsymbol{v}\big). \tag{14}$$

An axially symmetric body is then characterized by having $\boldsymbol{r}_\varphi = \boldsymbol{r}$. We further denote by $\mathscr{B}^-$ the body obtained from $\mathscr{B}$ by the reflection $\mathbf{R}_e$ about the plane orthogonal to $\boldsymbol{e}$ passing through the centroid of $\mathscr{B}$. For a body $\mathscr{B} \in \mathscr{K}^+$, $\mathscr{B}^-$ is represented by the radial mapping

$$\boldsymbol{r}^-(\boldsymbol{v}) := \mathbf{R}_e \boldsymbol{r}(\mathbf{R}_e \boldsymbol{v}).$$

We now show that for an axially symmetric body $\mathscr{B} \in \mathscr{K}^+$, $\boldsymbol{r}^* = \boldsymbol{r}^-$, which amounts to saying that the inverse $\mathscr{B}^*$ coincides with the mirror image $\mathscr{B}^-$. The formal proof of this fact is contained in the following chain of equalities:

$$\boldsymbol{r}^*(\boldsymbol{v}) = -\mathbf{R}_e^2 \boldsymbol{r}\big(-\mathbf{R}_e^2\boldsymbol{v}\big) = \mathbf{Q}_\pi \mathbf{R}_e \boldsymbol{r}\big(\mathbf{Q}_\pi^{\mathsf{T}}\mathbf{R}_e\boldsymbol{v}\big) = \boldsymbol{r}^-(\boldsymbol{v}), \tag{15}$$

where use has also been made of (13) and (14).

Suppose that $\mathscr{B}_1$ and $\mathscr{B}_2$ are axially symmetric bodies of $\mathscr{K}^+$ around the same axis $\boldsymbol{e}$. By (15), since $\mathscr{B}_2^-$ is also axially symmetric about $\boldsymbol{e}$, we obtain from (3) that

$$\boldsymbol{r}_e\big(\mathbf{Q}_\varphi^{\mathsf{T}}\boldsymbol{v}\big) = \boldsymbol{r}_1\big(\mathbf{Q}_\varphi^{\mathsf{T}}\boldsymbol{v}\big) + \boldsymbol{r}_2^-\big(\mathbf{Q}_\varphi^{\mathsf{T}}\boldsymbol{v}\big) = \mathbf{Q}_\varphi^{\mathsf{T}}\boldsymbol{r}_e(\boldsymbol{v}),$$

which proves that the excluded body of two axially symmetric bodies with the same symmetry axis is (maybe not surprisingly) axially symmetric too. Since $\boldsymbol{r}^{**} = \boldsymbol{r}$ and $\boldsymbol{r}^{--} = \boldsymbol{r}$, (15) also implies that $\boldsymbol{r}^{-*} = \boldsymbol{r}$. This latter has an important consequence. For any two bodies $\mathscr{B}_1,\mathscr{B}_2 \in \mathscr{K}^+$ axially symmetric about the same axis, $\mathscr{B}_e\{\mathscr{B}_1,\mathscr{B}_2^-\} = \mathscr{B}_1 + \mathscr{B}_2$. In particular, when $\mathscr{B}_1 = \mathscr{B}_2 = \mathscr{B}$, $\mathscr{B}_e\{\mathscr{B},\mathscr{B}^-\} = 2\mathscr{B}$, and so by (A52)

$$V_e\{\mathscr{B},\mathscr{B}^-\} = 8V[\mathscr{B}], \tag{16}$$

which is not to be confused with (9).

4. Symmetry group

Collecting the remarks made above in this section, we wish to identify here the most general symmetry group of $\mathscr{B}_e\{\mathscr{B}_1,\mathscr{B}_2\}$ when $\mathscr{B}_1$ and $\mathscr{B}_2$ are axially symmetric bodies, but not around the same axis. As above, we imagine the centroids c_1 and c_2 of $\mathscr{B}_1$ and $\mathscr{B}_2$ brought to coincide at one and the same point. Let $\boldsymbol{e}_1$ and $\boldsymbol{e}_2$ be the unit vectors designating their axes and let

$$\boldsymbol{e}_\perp = \frac{\boldsymbol{e}_1 \times \boldsymbol{e}_2}{|\boldsymbol{e}_1 \times \boldsymbol{e}_2|}$$

be the unit vector orthogonal to the plane spanned by $(\boldsymbol{e}_1,\boldsymbol{e}_2)$. Both $\mathscr{B}_1$ and $\mathscr{B}_2$ are mirror symmetric through $\boldsymbol{e}_\perp$, and so is then also $\mathscr{B}_e\{\mathscr{B}_1,\mathscr{B}_2\}$.

Moreover, let

$$\boldsymbol{e} = \frac{1}{\sqrt{2}}(\boldsymbol{e}_1 + \boldsymbol{e}_2)$$

[4] In general, the notation $\mathbf{Q}\{\mathscr{B}\}$ will be used for the body $\mathscr{B}$ transformed through the action of any orthogonal tensor $\mathbf{Q}$, not necessarily proper [see also Eq. (A53) below].

be the unit vector along the axis that bisects the axes of $\boldsymbol{e}_1$ and $\boldsymbol{e}_2$, all through the common centroid of the superimposed bodies. By applying to both $\mathscr{B}_1$ and $\mathscr{B}_2$ the rotation $\mathbf{Q}_\pi$ in (12), we exchange the bodies, so that, by (5),

$$\mathscr{B}_e\{\mathbf{Q}_\pi\{\mathscr{B}_1\},\mathbf{Q}_\pi\{\mathscr{B}_2\}\} = \mathscr{B}_e\{\mathscr{B}_2,\mathscr{B}_1\} = \mathscr{B}_e\{\mathscr{B}_1,\mathscr{B}_2\}^*. \tag{17}$$

Since, by combining (3) and (14), one easily proves that

$$\mathscr{B}_e\{\mathbf{Q}_\pi\{\mathscr{B}_1\},\mathbf{Q}_\pi\{\mathscr{B}_2\}\} = \mathbf{Q}_\pi\{\mathscr{B}_e\{\mathscr{B}_1,\mathscr{B}_2\}\},$$

(17) and (5) lead us to

$$\mathscr{B}_e\{\mathscr{B}_1,\mathscr{B}_2\} = \mathbf{Q}_\pi\{\mathscr{B}_e\{\mathscr{B}_1,\mathscr{B}_2\}\}^* = \mathbf{R}_{\boldsymbol{e}}\{\mathscr{B}_e\{\mathscr{B}_1,\mathscr{B}_2\}\},$$

showing that $\mathbf{R}_{\boldsymbol{e}}$, besides $\mathbf{R}_\perp$, is a symmetry transformation for $\mathscr{B}_e\{\mathscr{B}_1,\mathscr{B}_2\}$. It is now an easy exercise to see that

$$\mathbf{R}_\perp\mathbf{R}_{\boldsymbol{e}} = \mathbf{R}_{\boldsymbol{e}}\mathbf{R}_\perp = -\mathbf{R}^\perp := -(\mathbf{I} - 2\boldsymbol{e}^\perp \otimes \boldsymbol{e}^\perp),$$

where

$$\boldsymbol{e}^\perp := \frac{1}{\sqrt{2}}(\boldsymbol{e}_1 - \boldsymbol{e}_2).$$

In summary, the symmetry group of $\mathscr{B}_e\{\mathscr{B}_1,\mathscr{B}_2\}$ is composed of two reflections, $\mathbf{R}_{\boldsymbol{e}}$ and $\mathbf{R}_\perp$, through planes at right angles to one another, perpendicular to $\boldsymbol{e}$ and $\boldsymbol{e}_\perp$, and one π rotation, $-\mathbf{R}^\perp$, about the axis common to the planes of mirror symmetry. In Schönflies notation, this group is represented as

$$\mathsf{C}_{2v} := \{\mathbf{I},\mathbf{R}_{\boldsymbol{e}},\mathbf{R}_\perp, -\mathbf{R}^\perp\}.$$

III. OCTUPOLAR INTERPOLANT

In this section, we propose and justify an approximate formula for the excluded volume of two axially symmetric, convex bodies. In particular, we are interested in the simplest formula computable in terms of basic geometric functionals. We follow the example set forth by Straley [23] for the excluded volume of platelets in constructing our approximation as an interpolation between excluded volumes that can be computed exactly (see also [24] for the application of a similar method to approximate the Hamiltonian of hard dipolar spheres). In addition, we require the approximation to deliver exactly the isotropic average of the excluded volume, which within the Brunn-Minkowski theory for convex bodies is computed explicitly through (8).

Keeping these criteria in mind, we wish now to characterize the *shape* of a body by a number of tensors, to be used as descriptors of the bodies in the formula for their excluded volume. We sought guidance in the multipole expansion for the electromagnetic potential [as described, for example, in [25] (Sec. 3.1)], as the gravitational potential generated by a *mass* distribution has precisely the same mathematical form. The *shape tensors* of a body $\mathscr{B}$ will be those corresponding to a *uniform* mass density. There is only one important difference between the shape tensors thus defined and the usual multipole tensors. The former do not include a *dipole* moment, as this would be defined as

$$\boldsymbol{d}[\mathscr{B}] := \frac{1}{V[\mathscr{B}]}\int_{\mathscr{B}} (p - o)dv(p), \tag{18}$$

which coincides with the vector that in (A47) identifies the centroid c of $\mathscr{B}$, By choosing $o = c$ in (18), we set $\boldsymbol{d}[\mathscr{B}] \equiv \mathbf{0}$ and normalize all other multipolar shape tensors, referring them to c. To capture any sign of shape polarity, our theory must thus contemplate at least the *octupolar* shape tensor of a body $\mathscr{B}$.

The quadrupolar and octupolar shape tensors are defined as

$$\mathbf{q}[\mathscr{B}] := \frac{1}{V[\mathscr{B}]}\overline{\int_{\mathscr{B}} \boldsymbol{r}_c \otimes \boldsymbol{r}_c dv}\,, \tag{19}$$

$$\mathbf{t}[\mathscr{B}] := \frac{1}{V[\mathscr{B}]}\overline{\int_{\mathscr{B}} \boldsymbol{r}_c \otimes \boldsymbol{r}_c \otimes \boldsymbol{r}_c dv}\,, \tag{20}$$

where $\boldsymbol{r}_c := p - c$ is the position vector relative to the centroid c of $\mathscr{B}$ and the bracket $\overline{\cdots}$ extracts the fully symmetric, traceless component of the tensor it surmounts. For a body $\mathscr{B}$ axially symmetric about the unit vector $\boldsymbol{e}$, symmetry demands that [26]

$$\mathbf{q}[\mathscr{B}] = q[\mathscr{B}]\,\overline{\boldsymbol{e}\otimes\boldsymbol{e}}\,, \qquad \mathbf{t}[\mathscr{B}] = t[\mathscr{B}]\,\overline{\boldsymbol{e}\otimes\boldsymbol{e}\otimes\boldsymbol{e}}\,, \tag{21}$$

where

$$\begin{aligned}\overline{\boldsymbol{e}\otimes\boldsymbol{e}} &= \boldsymbol{e}\otimes\boldsymbol{e} - \tfrac{1}{3}\mathbf{I},\\ \overline{\boldsymbol{e}\otimes\boldsymbol{e}\otimes\boldsymbol{e}} &= \boldsymbol{e}\otimes\boldsymbol{e}\otimes\boldsymbol{e} - \tfrac{1}{5}\mathbb{E}\end{aligned} \tag{22}$$

and the third-rank tensor $\mathbb{E}$ has the following components in a Cartesian frame $(\boldsymbol{e}_1,\boldsymbol{e}_2,\boldsymbol{e}_3)$:

$$E_{ijk} = e_i\delta_{jk} + e_j\delta_{ki} + e_k\delta_{ij}, \tag{23}$$

where e_i are the components of $\boldsymbol{e}$. By use of (22) and (23), combining (21) with (18) leads us to the following expressions for the quadrupolar and octupolar shape *scalar moments* of $\mathscr{B}$:

$$q[\mathscr{B}] = \frac{1}{V[\mathscr{B}]}\int_{\mathscr{B}} r_c^2 P_2(\boldsymbol{e}_c\cdot\boldsymbol{e})dv, \tag{24}$$

$$t[\mathscr{B}] = \frac{1}{V[\mathscr{B}]}\int_{\mathscr{B}} r_c^3 P_3(\boldsymbol{e}_c\cdot\boldsymbol{e})dv, \tag{25}$$

where $\boldsymbol{r}_c$ has been represented as $\boldsymbol{r}_c = r_c\boldsymbol{e}_c$, with $\boldsymbol{e}_c$ a unit vector, and P_2 and P_3 are the Legendre polynomials

$$P_2(x) := \tfrac{1}{2}(3x^2 - 1) \quad \text{and} \quad P_3(x) := \tfrac{1}{2}(5x^2 - 3x).$$

Higher shape multipoles of order $n \geqq 4$ for an axially symmetric body $\mathscr{B}$ are easily recognized to be proportional to $\overline{\underbrace{\boldsymbol{e}\otimes\boldsymbol{e}\otimes\cdots\otimes\boldsymbol{e}}_{n\text{ times}}}$ through the scalar moment

$$m^{(n)}[\mathscr{B}] = \frac{1}{V[\mathscr{B}]}\int_{\mathscr{B}} r_c^n P_n(\boldsymbol{e}_c\cdot\boldsymbol{e})dv, \tag{26}$$

where P_n is the Legendre polynomial of degree n.

The excluded volume $V_e\{\mathscr{B}_1,\mathscr{B}_2\}$ of two axially symmetric bodies $\mathscr{B}_1$ and $\mathscr{B}_2$ must be invariant under both overall rotations of both bodies and rotations of each body about its symmetry axis. Moreover, as already remarked in the preceding section, $V_e\{\mathscr{B}_1,\mathscr{B}_2\}$ must be symmetric under the exchange of bodies. Letting $\boldsymbol{e}_1$ and $\boldsymbol{e}_2$ denote the unit vectors along the axes of symmetry of $\mathscr{B}_1$ and $\mathscr{B}_2$, respectively, all the above symmetry requirements impose that $V_e\{\mathscr{B}_1,\mathscr{B}_2\}$ be an isotropic, symmetric function $F(\boldsymbol{e}_1,\boldsymbol{e}_2)$ of the unit vectors

$\boldsymbol{e}_1$ and $\boldsymbol{e}_2$. In addition, and more importantly, we require that the approximation to F that we want to construct should result from an invariant combination of shape multipoles characterizing the bodies. Since a shape *dipole* is not contemplated in our formalism, as it would fail to be intrinsic, and higher multipoles have the form indicated in (19), (20), and (26) for the symmetry under study, we arrive at the following truncated approximation:

$$V_{\mathrm{e}}\{\mathscr{B}_1,\mathscr{B}_2\} = A + B\,\overline{\boldsymbol{e}_1\otimes\boldsymbol{e}_1}\cdot\overline{\boldsymbol{e}_2\otimes\boldsymbol{e}_2} + C\,\overline{\boldsymbol{e}_1\otimes\boldsymbol{e}_1\otimes\boldsymbol{e}_1}\cdot\overline{\boldsymbol{e}_2\otimes\boldsymbol{e}_2\otimes\boldsymbol{e}_2}, \quad (27)$$

where only the octupolar term has been retained of all possible higher moments, as it is the first capable in our theory of capturing the effects of shape polarity. The scalar coefficients A, B, and C are determined by requiring (27) to reproduce the exact excluded volume V_{e}^{+} in the *parallel* configuration, where $\boldsymbol{e}_1 = \boldsymbol{e}_2$, the excluded volume V_{e}^{-} in the *antiparallel* configuration, where $\boldsymbol{e}_1 = -\boldsymbol{e}_2$, and the *isotropic* average $\langle V_{\mathrm{e}}\rangle$, which the Brunn-Minkowski theory allows one to compute exactly through formula (8). Since

$$\overline{\boldsymbol{e}_1\otimes\boldsymbol{e}_1}\cdot\overline{\boldsymbol{e}_2\otimes\boldsymbol{e}_2} = \tfrac{2}{3}P_2(\boldsymbol{e}_1\cdot\boldsymbol{e}_2),$$
$$\overline{\boldsymbol{e}_1\otimes\boldsymbol{e}_1\otimes\boldsymbol{e}_1}\cdot\overline{\boldsymbol{e}_2\otimes\boldsymbol{e}_2\otimes\boldsymbol{e}_2} = \tfrac{2}{5}P_3(\boldsymbol{e}_1\cdot\boldsymbol{e}_2),$$

we easily arrive at

$$V_{\mathrm{e}} = \langle V_{\mathrm{e}}\rangle + \left[\tfrac{1}{2}(V_{\mathrm{e}}^{+}+V_{\mathrm{e}}^{-}) - \langle V_{\mathrm{e}}\rangle\right]P_2(\cos\theta) + \tfrac{1}{2}(V_{\mathrm{e}}^{+}-V_{\mathrm{e}}^{-})P_3(\cos\theta), \quad (28)$$

where we have set $\cos\theta := \boldsymbol{e}_1\cdot\boldsymbol{e}_2$.

IV. CIRCULAR CONES

We now compute both q and t for a circular cone $\mathscr{C}^{\alpha}$ with slant height L and semiamplitude α. The radius R and the height h of $\mathscr{C}^{\alpha}$ are $R = L\sin\alpha$ and $h = L\cos\alpha$, respectively [see Fig. 3(a)].

Letting o denote the center of the base, we easily find that the centroid c of $\mathscr{C}^{\alpha}$ is identified by $c - o = d\boldsymbol{e}$, where $\boldsymbol{e}$ is the unit vector along the axis and $d = \frac{1}{4}h$. Similarly, the volume V_{c} of $\mathscr{C}^{\alpha}$ is found to be [see also (A61b)]

$$V_{\mathrm{c}} = \tfrac{1}{3}\pi L\sin^2\alpha\cos\alpha. \quad (29)$$

Moreover, for $\mathscr{B} = \mathscr{C}^{\alpha}$ Eqs. (24) and (25), after a few computations, lead us to

$$q[\mathscr{C}^{\alpha}] = \tfrac{3}{80}L^2(5\cos^2\alpha - 4), \quad (30a)$$
$$t[\mathscr{C}^{\alpha}] = \tfrac{1}{160}L^3\cos\alpha(6 - 5\cos^2\alpha). \quad (30b)$$

It is perhaps interesting to remark that $t[\mathscr{C}^{\alpha}] > 0$ in the whole interval $0^\circ \leqq \alpha \leqq 90^\circ$, whereas $q[\mathscr{C}^{\alpha}]$ vanishes for $\alpha = \arctan\frac{1}{2} \doteq 26.6^\circ$, in which case $h = 2R$. Since when $q[\mathscr{C}^{\alpha}] = 0$ the first nonvanishing shape scalar multipole is $t[\mathscr{C}^{\alpha}]$, below we shall often consider this as the case of choice to illustrate our theory.

We now apply (28) to estimate the excluded volume of two congruent cones $\mathscr{C}^{\alpha}$ with axes making the angle θ. By (A35) and (A61a),

$$\langle V_{\mathrm{e}}\rangle = \frac{1}{2}\pi L^3\sin\alpha\left\{\left[\left(\frac{\pi}{2}+\alpha\right)\sin\alpha + \cos\alpha\right](1+\sin\alpha) + \frac{4}{3}\cos\alpha\sin\alpha\right\},$$

while $V_{\mathrm{e}}^{-} = 8V_{\mathrm{c}}$ by (16), and $V_{\mathrm{e}}^{+} = 14V_{\mathrm{c}}$ as a consequence of applying the Pappus-Guldinus theorem to the plane cross section in Fig. 3(b) whose rotation generates $\mathscr{B}_{\mathrm{e}}\{\mathscr{C}^{\alpha},\mathscr{C}^{\alpha}\}$, by the symmetry properties derived in Sec. II A3. With the aid of these relations we obtain from (28) the following interpolation formula for the excluded volume of a pair of cones:

$$v_{\mathrm{e}} = \langle v_{\mathrm{e}}\rangle + (11 - \langle v_{\mathrm{e}}\rangle)P_2(\cos\theta) + 3P_3(\cos\theta), \quad (31)$$

where $\langle v_{\mathrm{e}}\rangle$ is the isotropic average $\langle V_{\mathrm{e}}\rangle$ scaled to the volume V_{c} of $\mathscr{C}^{\alpha}$ in (29); explicitly,

$$\langle v_{\mathrm{e}}\rangle = 2 + \frac{3}{2}\frac{\left[\left(\frac{\pi}{2}+\alpha\right)\sin\alpha + \cos\alpha\right](1+\sin\alpha)}{\sin\alpha\cos\alpha}. \quad (32)$$

Figure 4 shows the graph of $\langle v_{\mathrm{e}}\rangle$ against α.

It grows indefinitely for both $\alpha \to 0^\circ$ and $\alpha \to 90^\circ$ and it attains its minimum $\langle v_{\mathrm{e}}\rangle_{\min} \doteq 11.8$ at $\alpha = \alpha_0 \doteq 25.2^\circ$. We recall that the shape quadrupole q of $\mathscr{C}^{\alpha}$ vanishes for $\alpha = \arctan(\frac{1}{2}) \doteq 26.6^\circ$. For every $\langle v_{\mathrm{e}}\rangle > \langle v_{\mathrm{e}}\rangle_{\min}$, there are precisely two values of the cone's semiamplitude that realize that same value of the isotropic average of the excluded volume. In each of the intervals $0^\circ < \alpha \leqq \alpha_0$ and $\alpha_0 \leqq \alpha < 90^\circ$, $\langle v_{\mathrm{e}}\rangle$ could be taken as an alternative parameter for $\mathscr{C}^{\alpha}$, to which one and the same excluded volume would correspond through (31). Said differently, (31) assigns one and the same

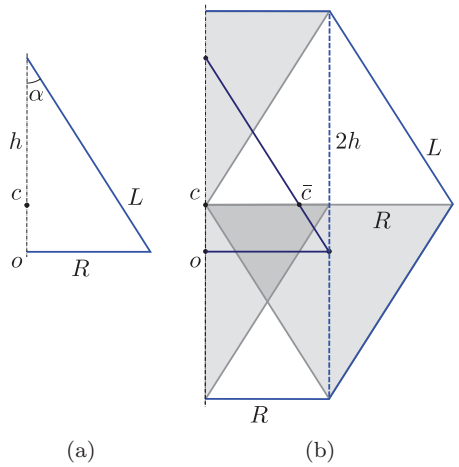

FIG. 3. (Color online) (a) The triangle whose rotation about $\boldsymbol{e}$ by the angle 2π generates the circular cone $\mathscr{C}^{\alpha}$ with slant height L and semiamplitude α. $R = L\sin\alpha$ is the radius of $\mathscr{C}^{\alpha}$, $h = L\cos\alpha$ is its height, and $d = h/4$ is the distance of the centroid c of $\mathscr{C}^{\alpha}$ from the center o of its base. (b) The polygon whose rotation about $\boldsymbol{e}$ by the angle 2π generates the excluded body $\mathscr{B}_{\mathrm{e}}\{\mathscr{C}^{\alpha},\mathscr{C}^{\alpha}\}$ of two congruent cones in the parallel configuration. It is a rectangle of sides $2h$ and R flanked by an isosceles triangle of base $2h$ and height R. Here $\bar{c}$ is the centroid of the generating polygon and $\bar{d} = 7R/9$ is its distance from the centroid c of $\mathscr{B}_{\mathrm{e}}\{\mathscr{C}^{\alpha},\mathscr{C}^{\alpha}\}$ on the axis of rotation. The shaded triangles represent the cross sections of the central inverse of $\mathscr{C}^{\alpha}$ in the construction of $\mathscr{B}_{\mathrm{e}}\{\mathscr{C}^{\alpha},\mathscr{C}^{\alpha}\}$ outlined in Fig. 2.

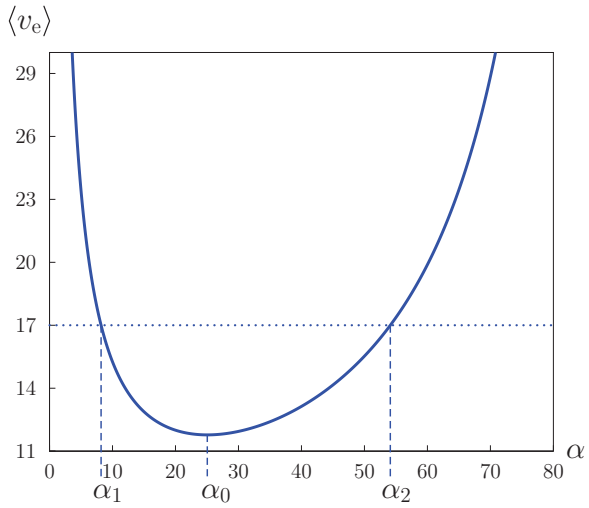

FIG. 4. (Color online) Plot of the isotropic average of the excluded volume of two congruent cones with semiamplitude α, scaled to the cone's volume V_c in (29). The function $\langle v_e \rangle$ in (32) attains its minimum $\langle v_e \rangle_{min} \doteq 11.8$ at $\alpha_0 \doteq 25.2^\circ$. The special value $\langle v_e \rangle = 17$ is attained at both $\alpha_1 \doteq 8.02^\circ$ and $\alpha_2 \doteq 53.9^\circ$.

scaled excluded volume to the two cones that have one and the same isotropic excluded volume average.

Figure 5 shows three graphs of the scaled excluded volume v_e in (31) (for three different values of $\langle v_e \rangle$) against the angle θ which represents the relative orientation of the two cones: $\theta = 0^\circ$ corresponds to the parallel configuration, whereas $\theta = 180^\circ$ corresponds to the antiparallel configuration. A few remarks are suggested by the analysis of the function v_e. First, v_e attains its absolute minimum in the antiparallel configuration, for all values of $\langle v_e \rangle$, confirming for cones a result already found

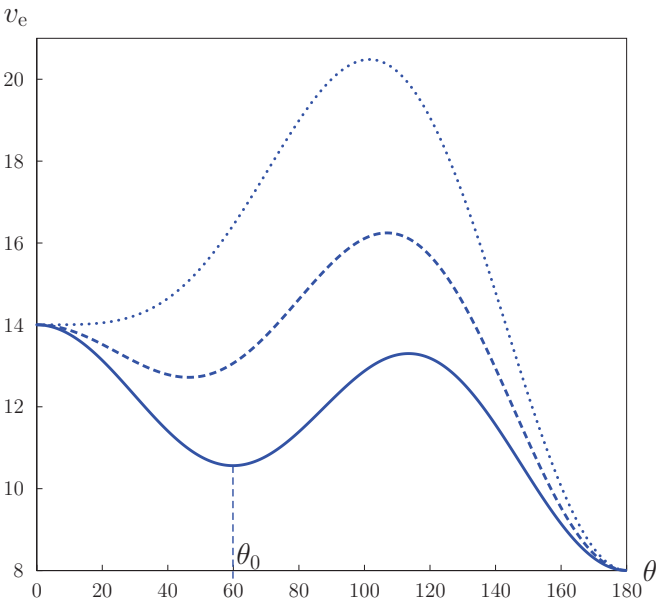

FIG. 5. (Color online) The graphs of v_e against θ (expressed in degrees) for three different values of $\langle v_e \rangle$, namely, $\langle v_e \rangle = \langle v_e \rangle_{min}$ (solid line), $\langle v_e \rangle = 14$ (dashed line), and $\langle v_e \rangle = 17$ (dotted line). The relative minimum which falls at $0^\circ < \theta_0 < 180^\circ$ retreats towards 0° as $\langle v_e \rangle$ increases towards 17.

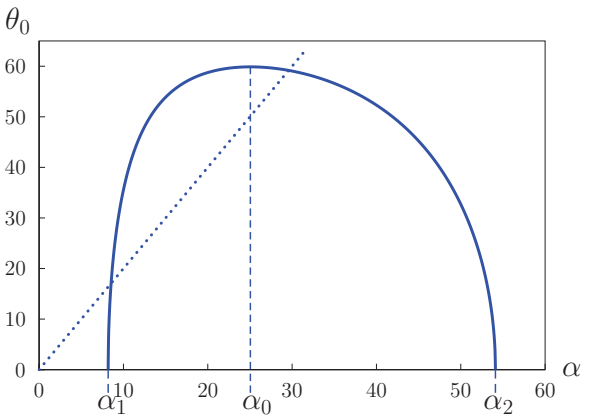

FIG. 6. (Color online) The value θ_0 of θ where v_e attains its relative minimum is shown as a function of α in the interval $[\alpha_1,\alpha_2]$ identified in Fig. 4. The maximum of this function, which is attained at $\alpha = \alpha_0$, is $\theta_0 \doteq 60.2^\circ$. The dotted line, corresponding to $\theta = 2\alpha$, is drawn for a comparison: it represents the relative inclination of the cones at which they would slide along a common slant height.

for V-shaped rods in two space dimensions [27]. Second, for $\langle v_e \rangle_{min} \leqq \langle v_e \rangle \leqq 17$, v_e attains a relative minimum at $\theta = \theta_0$, with $0^\circ < \theta_0 < 180^\circ$, which, as shown in Fig. 5, deepens as $\langle v_e \rangle$ approaches $\langle v_e \rangle_{min}$.[5] Third, for $\langle v_e \rangle > 17$, the relative minimum of v_e falls in the parallel configuration, and the maximum separating it from the absolute minimum in the antiparallel configuration increases with increasing $\langle v_e \rangle$. Figure 6 illustrates how θ_0 depends on α in the interval $[\alpha_1,\alpha_2]$; its maximum is attained for $\alpha = \alpha_0$.

Despite its possible suggestiveness, Eq. (31) represents just an approximation to the excluded volume of two cones, which calls for a justification stronger than our argument above might convey. In the following section, we shall apply a shape-reconstruction algorithm to generate the excluded body of two regularized cones, for which we shall compute numerically the excluded volume and compare it to the one delivered by (31).

V. SPHEROCONES

To smooth a cone and make its shape amenable to an accurate computer-aided reconstruction, we transform it into a *spherocone*. In general, as explained in Appendix A 1, for a convex body $\mathscr{B}$, the *spherobody* $\mathscr{B}_r$ is obtained by the (Minkowski) addition to $\mathscr{B}$ of a ball of radius r. In the kinematic metaphor susggested by Fig. 1, $\partial\mathscr{B}_r$ is generated by the center of a ball of radius r that slides on $\partial\mathscr{B}$. The mean curvature M, the area surface S, and the volume V of $\mathscr{B}_r$ are related to the corresponding values of these functional for $\mathscr{B}$ through Eqs. (A26), (A44), and (A51), respectively. Specifically, for a spherocone $\mathscr{C}_r^\alpha$ these formulas take the form in (A62). As noted in Appendix A 6, a spherocone $\mathscr{C}_r^\alpha$ becomes a spherorod $\mathscr{R}_r$ or a spherodisk $\mathscr{D}_r$, by setting $\alpha = 0^\circ$ or $\alpha = 90^\circ$, respectively.

[5]The special value $\langle v_e \rangle = 17$ is identified by requiring the second derivative of v_e in (31) to vanish at $\theta = 0^\circ$.

FIG. 7. A spherocone $\mathscr{C}_r^\alpha$ with $\alpha = \arctan(1/2) \doteq 26.6^\circ$ and $r = L/10$.

For a spherocone $\mathscr{C}_r^\alpha$, we shall scale r to the slant height L of $\mathscr{C}^\alpha$, introducing the parameter

$$\varrho := \frac{r}{L}.$$

A spherocone with $\alpha = \arctan\frac{1}{2} \doteq 26.6^\circ$ is shown in Fig. 7. By (A62c), the volume $V_{\rm sc}$ of $\mathscr{C}_r^\alpha$ is then expressed by

$$\frac{V_{\rm sc}}{L^3} = \frac{4\pi}{3}\varrho^3 + \pi\varrho^2\left[\left(\frac{\pi}{2}+\alpha\right)\sin\alpha + \cos\alpha\right] + \pi\varrho\sin\alpha(1+\sin\alpha) + \frac{1}{3}\pi\sin^2\alpha\cos\alpha, \quad (33)$$

which parallels (29). Similarly, by combining (A58) and (A62), we write the isotropic average $\langle V_{\rm e}\rangle$ of the excluded volume of two congruent spherocones as

$$\frac{\langle V_{\rm e}\rangle}{L^3} = \frac{32}{3}\pi\varrho^3 + 8\pi\varrho^2\left[\left(\frac{\pi}{2}+\alpha\right)\sin\alpha + \cos\alpha\right] + \pi\varrho \times\left\{4\sin\alpha(1+\sin\alpha) + \left[\left(\frac{\pi}{2}+\alpha\right)\sin\alpha + \cos\alpha\right]^2\right\} + \frac{1}{2}\pi\sin\alpha\left\{\left[\left(\frac{\pi}{2}+\alpha\right)\sin\alpha + \cos\alpha\right](1+\sin\alpha) + \frac{4}{3}\cos\alpha\sin\alpha\right\}. \quad (34)$$

A construction similar to the one that in Fig. 3(b) led us to compute the excluded volume of $V_{\rm e}^+$ of two cones in the parallel configuration here delivers the following expression:

$$\frac{V_{\rm e}^+}{L^3} = \frac{32}{3}\pi\varrho^3 + 8\pi\varrho^2\left[\left(\frac{\pi}{2}+\alpha\right)\sin\alpha + \cos\alpha\right] + 4\pi\varrho\sin\alpha(3+\sin\alpha) + \frac{14}{3}\pi\sin^2\alpha\cos\alpha, \quad (35)$$

while, by general symmetry properties, we still have that the excluded volume of two spherocones in the antiparallel configuration is $V_{\rm e}^- = 8V_{\rm sc}$.

With the aid of these formulas, we can easily form the isotropic average of the excluded volume $\langle v_{\rm e}\rangle$ scaled to $V_{\rm sc}$, which is depicted in Fig. 8 for three values of ϱ. For given ϱ, $\langle v_{\rm e}\rangle$ is a function of α, bounded in the whole interval $0^\circ \leqq \alpha \leqq 90^\circ$, which exhibits an isolated minimum at $\alpha = \alpha_0(\varrho)$; α_0 moderately increases with ϱ, approaching $\alpha_0 \doteq 29.8^\circ$ as $\varrho \gg 1$. In this asymptotic limit, $\langle v_{\rm e}\rangle$ plummets to the constant $\langle v_{\rm e}\rangle \equiv 8$, characteristic of a sphere. For any finite $\varrho > 0$, the value of $\langle v_{\rm e}\rangle$ at $\alpha = 90^\circ$ is larger than the value of $\langle v_{\rm e}\rangle$ at $\alpha = 0^\circ$, in keeping with the intuitive view that spherodisks are on average less accommodating than spherorods with the same volume.

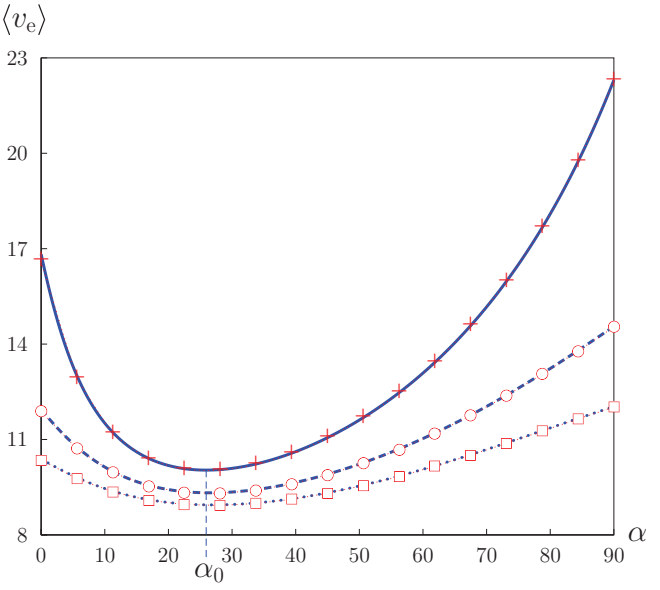

FIG. 8. (Color online) The isotropic average $\langle v_{\rm e}\rangle$ of the excluded volume of two spherocones $\mathscr{C}_r^\alpha$ scaled to $V_{\rm sc}$ according to (33) and (34) shown as a function of α (expressed in degrees), for three values of $\varrho = r/L$, namely, $\varrho = 0.1$ (solid line), $\varrho = 0.2$ (dashed line), and $\varrho = 0.3$ (dotted line). The function $\langle v_{\rm e}\rangle$ attains its minimum at $\alpha = \alpha_0(\varrho)$; here $\alpha_0(0.1) \doteq 25.8^\circ$, $\alpha_0(0.2) \doteq 26.4^\circ$, and $\alpha_0(0.3) \doteq 26.9^\circ$. As ϱ increases, $\langle v_{\rm e}\rangle$ monotonically collapses towards the constant $\langle v_{\rm e}\rangle \equiv 8$. Crosses, circles, and squares (red online) identify the values of the isotropic average $\langle v_{\rm e}\rangle$ computed numerically with the method in Appendix B, for $\varrho = 0.1$, $\varrho = 0.2$, and $\varrho = 0.3$, respectively.

For spherocones, the excluded volume $V_{\rm e}^+$ is not a multiple of $V_{\rm sc}$ independent of α and ϱ, and so (28), once expressed as the excluded volume $v_{\rm e}$ of two congruent spherocones scaled to $V_{\rm sc}$, can no longer be given the neat form in (31) that we obtained for cones. However, qualitatively $v_{\rm e}$ has the same features for both cones and spherocones. For every $\varrho > 0$, there are $\alpha_1(\varrho)$ and $\alpha_2(\varrho)$ such that for $\alpha_1(\varrho) < \alpha < \alpha_2(\varrho)$ the volume $v_{\rm e}$ attains a relative minimum at θ_0 in the open interval $0^\circ < \theta < 180^\circ$ (as well as a relative maximum), whereas for both $\alpha \geqq \alpha_2(\varrho)$ and $\alpha \leqq \alpha_1(\varrho)$ the function $v_{\rm e}$ only attains a relative maximum in the open interval $0^\circ < \theta < 180^\circ$ and has there no relative minimum.[6] For every $\varrho > 0$, the isotropic average $\langle v_{\rm e}\rangle$ is no longer the same for $\alpha = \alpha_1$ and $\alpha = \alpha_2$, but still the relative minimum of $v_{\rm e}$ is deepest for $\alpha = \alpha_0(\varrho)$. The functions $\alpha_1(\varrho)$ and $\alpha_2(\varrho)$ vary very slowly: α_1 increases steadily from $\alpha_1(0) \doteq 8.02^\circ$ to $\alpha_1^\infty \doteq 9.79^\circ$, whereas α_2 decreases steadily from $\alpha_2(0) \doteq 53.9^\circ$ to $\alpha_2^\infty \doteq 52.6^\circ$ as ϱ diverges to infinity (both α_1^∞ and α_2^∞ were determined by solving numerically a transcendental equation). Figure 9 illustrates the function $\theta_0(\varrho)$, which designates the deepest relative minimum of $v_{\rm e}$ [corresponding to the cone's semiamplitude $\alpha_0(\varrho)$].

[6] For given ϱ, $\alpha_1(\varrho)$ and $\alpha_2(\varrho)$ are obtained by requiring the second derivative of $v_{\rm e}$ to vanish at $\theta = 0^\circ$.

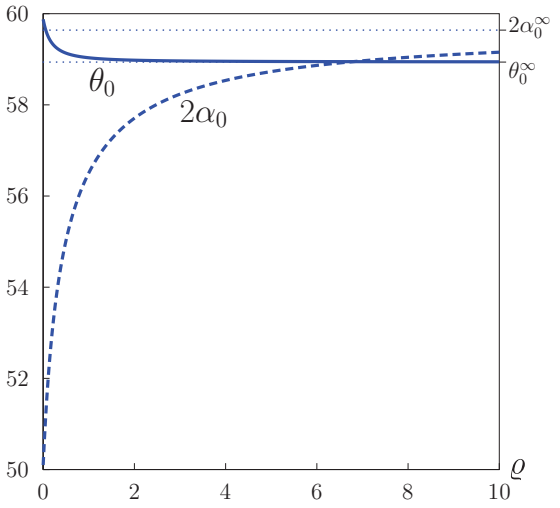

FIG. 9. (Color online) The graph of θ_0 (solid line) contrasted against the graph of $2\alpha_0$ (dashed line). Both converge to asymptotic values as $\varrho \to \infty$: $\theta_0^\infty \doteq 58.9^\circ$ and $2\alpha_0^\infty \doteq 59.6^\circ$. The comparison between these graphs supports the approximate relation $\theta_0 \approx 2\alpha_0$.

As ϱ increases, θ_0 decreases from $\theta_0(0) \doteq 60.2^\circ$ (see also Fig. 6) to $\theta_0^\infty \doteq 58.9^\circ$. In Fig. 9, the graph of θ_0 is also compared with the graph of the amplitude $2\alpha_0$ of the corresponding cone at which the isotropic average $\langle v_e \rangle$ attains its minimum. For most values of ϱ, these graphs are very close to one another, showing that the deepest local minimum in the excluded volume occurs when one spherocone slides with its slant height almost parallel to that of its companion.

Figure 10 illustrates the graph of v_e for spherocones with different values of ϱ; in all cases α is chosen as the corresponding $\alpha_0(\varrho)$. As $\langle v_e \rangle$ monotonically approaches $\langle v_e \rangle \equiv 8$ for increasing ϱ, so also does v_e.

For $\varrho > 0$ and α outside the interval $[\alpha_1, \alpha_2]$, the relative minimum of v_e falls in the parallel configuration ($\theta = 0^\circ$). In particular, in the limiting cases of a spherorod ($\alpha = 0^\circ$) and a spherodisk ($\alpha = 90^\circ$) the graph of v_e is symmetric about $\theta = 90^\circ$, where it attains its maximum. We record here, for a comparison, the explicit form that v_e takes for both a spherorod and a spherodisk:

$$v_e|_{\alpha=0^\circ} = 8 + \frac{9 \sin^2 \theta}{2\varrho(4\varrho + 3)}, \tag{36a}$$

$$v_e|_{\alpha=90^\circ} = 8 + \frac{9[(\pi^2 - 8)\varrho + \pi] \sin^2 \theta}{2\varrho(4\varrho^2 + 3\pi\varrho + 6)}. \tag{36b}$$

Equations (36) represent the *quadrupolar*, average-preserving approximations to the excluded volume for spherorods and spherodisks. For the former, the exact formula is known, that is,

$$v_e^{(\mathrm{sr})} := 8 + \frac{12 \sin \theta}{\pi\varrho(4\varrho + 3)}, \tag{36c}$$

[see, for example, Eq. (21) of [28]]. Figure 11 shows the plot of the relative error

$$\delta_e^{(\mathrm{sr})} := \frac{v_e|_{\alpha=0^\circ} - v_e^{(\mathrm{sr})}}{v_e^{(\mathrm{sr})}} = \frac{9\pi \sin\theta(3\pi \sin\theta - 8)}{8[2\pi\varrho(4\varrho + 3) + 3 \sin\theta]}, \tag{36d}$$

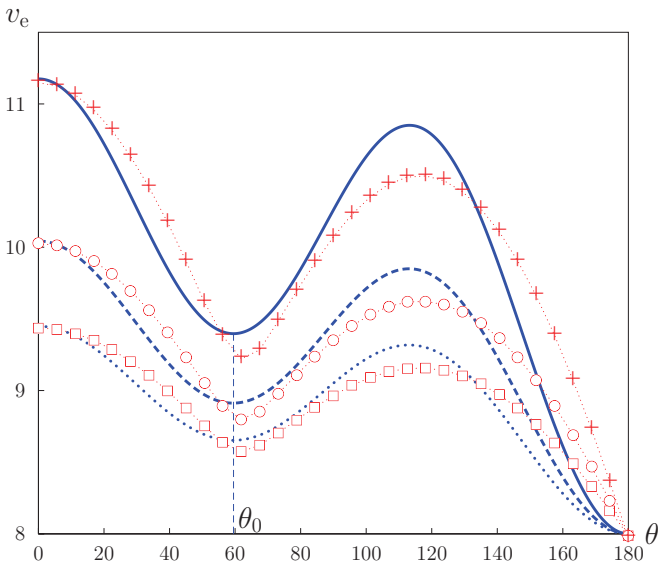

FIG. 10. (Color online) The scaled excluded volume v_e of two spherocones against the angle θ between the bodies' axes (expressed in degrees), for three values of ϱ, namely, $\varrho = 0.1$ (solid line), $\varrho = 0.2$ (dashed line), and $\varrho = 0.3$ (dotted line). In all three cases, the value chosen for α is $\alpha_0(\varrho)$, as in the caption to Fig. 8. The function v_e attains a relative minimum at $\theta_0(\varrho)$; here $\theta_0(0.1) \doteq 59.5^\circ$, $\theta_0(0.2) \doteq 59.4^\circ$, and $\theta_0(0.3) \doteq 59.2^\circ$. As ϱ increases, v_e monotonically collapses towards the constant $v_e \equiv 8$, characteristic of spheres. Crosses, circles, and squares (red online) identify the values of the isotropic average $\langle v_e \rangle$ computed numerically with the method in Appendix B, for $\varrho = 0.1$, $\varrho = 0.2$, and $\varrho = 0.3$, respectively.

which vanishes at $\theta = \arcsin(\frac{8}{3\pi}) \doteq 58.1^\circ$ and $\theta = 180^\circ - \arcsin(\frac{8}{3\pi}) \doteq 121.9^\circ$, for all values of ϱ.

The relatively modest agreement between (36a) and (36c) suggests that in general (28) fits better when its octupolar term does not vanish identically, that is, in the presence of shape polarity.[7]

The excluded body $\mathscr{B}_e$ of two congruent spherocones $\mathscr{C}_r^\alpha$ has been reconstructed by means of the algorithm outlined in Appendix B. Figure 12 illustrates the shape of $\mathscr{B}_e$ obtained for different values of the relative orientation angle θ when $\alpha = \arctan\frac{1}{2} \doteq 26.6^\circ$ and $\varrho = 0.1$.

The shapes of $\mathscr{B}_e$ obtained for several relative orientations of the two spherocones (as well as other parameters) are illustrated in the Supplemental Material [30]. All these shapes clearly display the C_{2v} symmetry anticipated in Sec. II A4.

For each of the reconstructed shapes of $\mathscr{B}_e$, the volume V_e was computed numerically as was its isotropic average $\langle V_e \rangle$. The exact form of the scaled isotropic average $\langle v_e \rangle$ was taken as a benchmark for our method. Figure 8 also shows the comparison between the computed and exact values of $\langle v_e \rangle$. The scaled excluded volume v_e, computed numerically, is similarly contrasted in Fig. 10 against the graph describing formula (28).

[7] An approximation to the excluded volume of two spherodisks which considerably improves (36b) will be presented elsewhere [29].

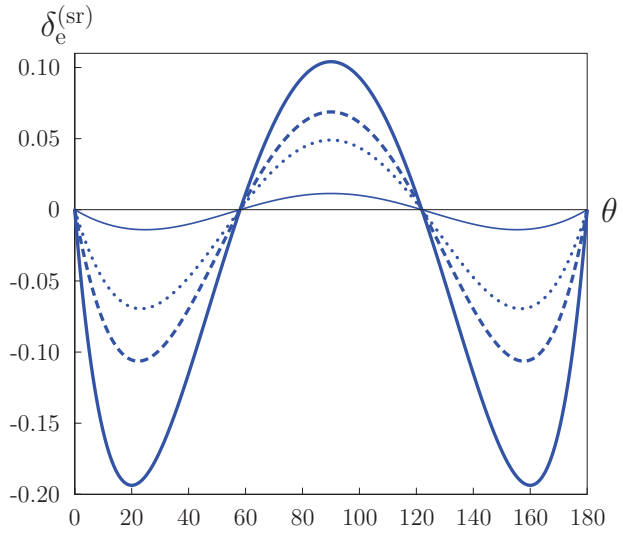

FIG. 11. (Color online) The function $\delta_e^{(sr)}$ defined as in (36d) represents the relative error between the quadrupolar approximation to the excluded volume of spherorods in (36a) and the exact formula in (36c). Here $\delta_e^{(sr)}$ is plotted against the angle θ made by the axes of the spherorods (expressed in degrees) for different values of the ratio $\varrho = r/L$ between the radius r of the sphere and the length L of the rod, namely, $\varrho = 0.1$ (solid line), $\varrho = 0.2$ (dashed line), $\varrho = 0.3$ (dotted line), and $\varrho = 1$ (thin solid line).

Paralleling (36d), we define for spherocones the relative error

$$\delta_e^{(sc)} := \frac{v_e - v_e^{(rec)}}{v_e^{(rec)}}, \tag{37}$$

where v_e is delivered by the octupolar approximation (28) and $v_e^{(rec)}$ is computed numerically on the shape reconstructed through the method described in Appendix B. Figure 13 illustrates the graph of $\delta_e^{(sc)}$ as a function of (α,θ) for $\varrho = 0.1$. As already expected from the behavior of $\delta_e^{(sr)}$ in Fig. 11, the octupolar approximation is not particularly successful for either spherorods ($\alpha = 0^\circ$) or spherodisks ($\alpha = 90^\circ$), but it improves considerably for true spherocones. We may say that the octupolar interpolation in (28) is fully satisfactory in the presence of shape polarity. In the following section, we shall comment further on the consequences that the predictions based on (28) may have for spherocones.

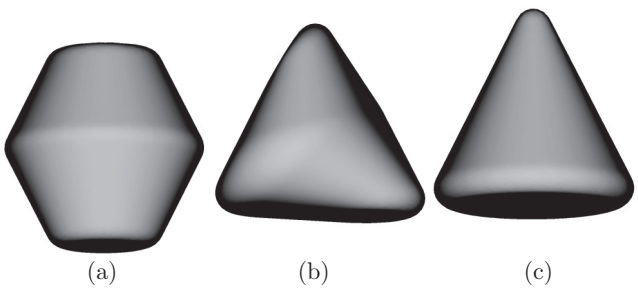

FIG. 12. The shapes of the excluded bodies for two congruent spherocones with $\alpha = \arctan(1/2) \doteq 26.6^\circ$ and $\varrho = 0.1$ at different orientation angles, namely, (a) $\theta = 0^\circ$, (b) $\theta = \theta_0(0.1) \doteq 59.3^\circ$, and (c) $\theta = 180^\circ$. The centroids of the three bodies are aligned for reference on one and the same horizontal line.

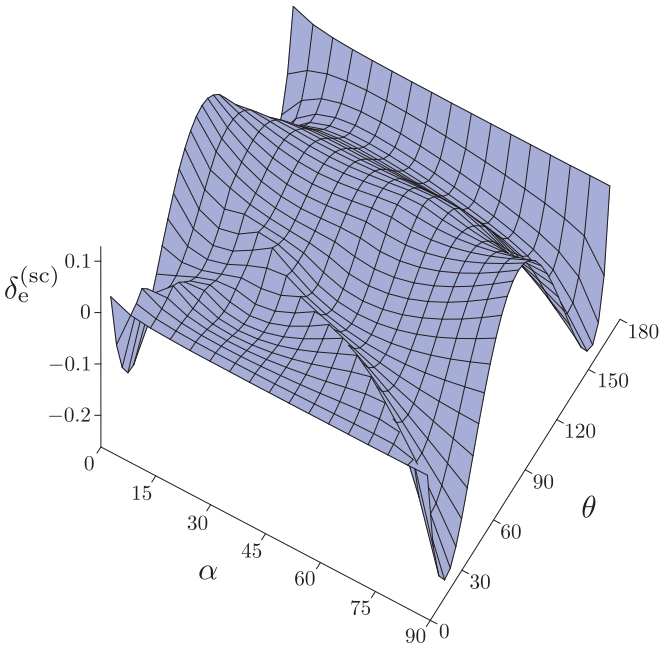

FIG. 13. (Color online) Plot of the relative error $\delta_e^{(sc)}$ defined in (37) for $\varrho = 0.1$. The values of $\delta_e^{(sc)}$ are computed on a 17×33 grid in the plane (α,θ), with a spacing of $(\pi/32)$ rad $\doteq 5.63^\circ$ along each direction. On this grid, $\delta_e^{(sc)}$ ranges in the interval $[-0.25,0.12]$ and the root mean square (rms) of all the values it takes is 0.065.

VI. CONCLUSION

We proposed an interpolation formula for the excluded volume of two convex, axially symmetric bodies, which involves at most the octupolar shape tensor assignable to each body. We argued that a shape dipole cannot be intrinsically ascribed to a body; accordingly, the octupolar term, which in (28) is represented by the Legendre polynomial P_3, is the lowest multipole capable of representing the effects of shape polarity in the excluded volume.

By applying the Brunn-Minkowski theory of convex bodies, which is amply recalled in Appendix A for the ease of the reader, we proved that the body excluded by the mutual presence of two convex, axially symmetric bodies enjoys at least the C_{2v} symmetry. Likewise, we showed that the excluded volume of two congruent such bodies in the antiparallel configuration equals eight times the volume of each single body.

We applied our theory to both cones and *spherocones*, which are cones smoothed by the (Minkowski) addition of a sphere. For these special bodies, we concluded that the excluded volume attains its absolute minimum in the antiparallel configuration, but a relative, deep minimum may also appear for an appropriate choice of parameters. These conclusions were further corroborated by applying a shape-reconstruction algorithm (described in some detail in Appendix B) which generated the excluded body of two congruent spherocones (a gallery of reconstructed shapes is also shown in the Supplemental Material [30]). The excluded volume that was then computed numerically confirmed the predictions based on the interpolation formula (28), raising our confidence in its general validity in the presence of shape polarity.

There are a number of lines of thought arising from this work that we would like to see further pursued. First, one could attempt to find an interpolating formula like (28) for less symmetric bodies. The first class of bodies that come to mind would be arc-shaped bodies, which fail to be convex, but possess at least the C_{2v} symmetry. For these bodies, an appropriate shape-reconstruction algorithm would be needed to benchmark an extended interpolant for the excluded volume.

Second, for spherocones, which here served the purpose of validating (28), the appearance of a relative minimum for the excluded volume suggests exploring further the behavior of a system of hard-core particles with such a shape, to probe the onset of possibly metastable equilibrium ordered arrangements different from the assembly in dimers suggested by the occurrence of the absolute minimum of the excluded volume in the antiparallel configuration. Choosing the cones' semiamplitude $\alpha = \alpha_0$, so as to minimize the isotropic excluded volume average, also makes the relative minimum at $\theta = \theta_0$ of the excluded volume the deepest. As shown in Fig. 9, θ_0 is close to the cones' amplitude $2\alpha_0$, so that they could be more easily locked in configurations where they nearly glide along a common slant height. Such peculiar configurations already occurred in the arrangements of some tapered convex particles interacting only through their shapes, which have been seen to generate a *gyroid*[8] minimum surface [32].

Third, a simple extension of the method of approximation presented here can be applied to the excluded volume of two different axially symmetric convex shapes. It might be instrumental in devising methods to optimize either the mixing or the demixing of different hard particles, such as cones and plates or cones and rods. Such a study is presently under way and will be presented elsewhere [33].

Finally, it would be desirable to extend our work to cover the steric corrections to attractive dispersion force interactions by computing for spherocones and other axially symmetric, convex bodies the steric tensor introduced in [21] (see also [34]). We think that all these issues might in general be relevant to the study of steric interactions in colloidal systems.

ACKNOWLEDGMENTS

We are grateful to the Italian MIUR for the financial support provided to this project through Grant No. PRIN 2009N5JH4F. E.G.V. acknowledges the kind hospitality of the Isaac Newton Institute in Cambridge, where this work was completed, and the support of the Institute as a Visiting Fellow participating in the program on The Mathematics of Liquid Crystals.

APPENDIX A: PRIMER ON CONVEX BODIES

In this Appendix we review classical results of convex geometry that can be found in many books, among which we mention the treatises [35–37], where all the elementary topics recalled here are presented, although at different levels of generality and formalization. The Brunn-Minkowski theory, as laid down in Brunn's dissertation [38] and in the subsequent work of Minkowski [19], lies at the heart of this primer. As effectively suggested in the Preface to [37], the Brunn-Minkowski theory results from merging two elementary notions in Euclidean spaces, namely, vector addition in the associated translation space and volume measure. The former operation, usually called the Minkowski addition, endows the class of all convex sets in a Euclidean space with a rich mathematical structure. When combined with the volume measure, this structure reveals significant links to both area and curvature measures through the *Minkowski functionals* (also known as the *Quermassintegrals*) and the *mixed volumes* (in this respect, see also the more recent book [39]). Below, these functionals will be simply designated as *curvature functionals*. The integral representation of these functionals constitutes the connection between geometric convexity and integral geometry, which was initiated in the late 1930s by Blaschke [40] (see also [36,37]).

Clearly, in the little room that we can afford here, we shall only touch upon a few elementary topics at the crossroad between different disciplines, which are essential to the development of the main body of the paper. In particular, we shall renounce dwelling on the deep relationships between Minkowski functionals, curvature measures, and mixed volumes. To make our presentation self-contained, we shall adopt a unified formalism, although our sources are disparate. For simplicity, we shall also confine our attention to convex bodies in three space dimensions, although the results recalled below are valid in higher dimensions, albeit in a more complicated formulation.

1. Basic definitions and theorems

Let $\mathscr{E}$ be the three-dimensional Euclidean space with associated translation space $\mathscr{V}$. We shall call a "body" any regularly open set $\mathscr{B}$ of $\mathscr{E}$, that is, any set that coincides with the interior of its closure.[9] A body $\mathscr{B} \subset \mathscr{E}$ is said to be *convex*, if for any pair of points (p_1, p_2) in $\mathscr{B}$, the point $p_\lambda := \lambda p_1 + (1-\lambda)p_2$ belongs to $\mathscr{B}$, for all $\lambda \in [0,1]$. In geometric terms, this means that the whole segment joining p_1 and p_2 is contained in $\mathscr{B}$. Moreover, a convex body $\mathscr{B}$ is said to be *strictly* convex, whenever for any pair (p_1, p_2) of points on $\partial\mathscr{B}$, the point $p_\lambda \notin \partial\mathscr{B}$ for all $\lambda \in]0,1[$. In geometric terms, this means that the boundary of a strictly convex body does not contain any segment. We shall denote by $\mathscr{K}$ the class of all convex bodies of $\mathscr{E}$.

Let $\mathscr{B}_1$ and $\mathscr{B}_2$ be bodies of $\mathscr{E}$. The Minkowski addition of $\mathscr{B}_1$ and $\mathscr{B}_2$ is the body operation defined by

$$\mathscr{B}_1 + \mathscr{B}_2 := \{p \in \mathscr{E} \,|\, p - o = (p_1 - o) + (p_2 - o), p_1 \in \mathscr{B}_1, p_2 \in \mathscr{B}_2\}, \tag{A1}$$

[8] See, for example, [31] for further mathematical details on a whole family of minimum surfaces of the same kind.

[9] Points of $\mathscr{E}$ are denoted as $o, p, \ldots$. For $p_1, p_2 \in \mathscr{E}$, the *vector* $(p_2 - p_1)$ is the translation of $\mathscr{V}$ that brings p_1 into p_2. The Euclidean distance between p_1 and p_2 is the *length* of the vector $(p_2 - p_1)$, defined as $|p_2 - p_1| := \sqrt{(p_2 - p_1)\cdot(p_2 - p_1)}$, where $\cdot$ denotes the inner product in $\mathscr{V}$. For the general mathematical setting for the Euclidean and associated translation spaces, we refer the reader to either of the recent books [34,41].

where o is any point in $\mathscr{E}$ taken as origin. The body $\mathscr{B}_1 + \mathscr{B}_2$ is also called the Minkowski sum of $\mathscr{B}_1$ and $\mathscr{B}_2$. Properly speaking, the definition in (A1) depends on the choice of o. However, by changing o into o' in (A1) $\mathscr{B}_1 + \mathscr{B}_2$ would be defined as the body

$$\{p' \in \mathscr{E} \,|\, p' - o' = (p_1 - o') + (p_2 - o'), p_1 \in \mathscr{B}_1, p_2 \in \mathscr{B}_2\},$$

which, since $(p' - o) = (p_1 - o) + (p_2 - o) + (o - o') = (p - o) + (o - o')$, differs from the body in (A1) only by the translation $(o - o')$. Thus, if o is set free, the set $\mathscr{B}_1 + \mathscr{B}_2$ is defined by (A1) to within a translation. In the following, a choice of o will be understood, with no prejudice to our development. In general, it is the same for all bodies; on occasion, it may be chosen to be different for different bodies, but this will always be noted.

Similarly, for any $\lambda \in \mathbb{R}$ the *scalar multiplication* of a body $\mathscr{B} \subset \mathscr{E}$ by λ relative to a point $o \in \mathscr{E}$ is defined by

$$\lambda\mathscr{B} := \{p' \in \mathscr{E} \,|\, (p' - o) = \lambda(p - o), p \in \mathscr{B}\}. \quad \text{(A2)}$$

The scalar multiple $\lambda\mathscr{B}$ of $\mathscr{B}$ clearly depends on the choice of the point o. Proceeding exactly as above, we easily prove that by changing o into o' we translate the body $\lambda\mathscr{B}$ by the vector $\lambda(o - o')$. For convenience, in the following we shall fix one and the same point o, relative to which both scalar multiplication and Minkowski addition of bodies are meant to be defined. Since in (A2) λ may also be negative, for $\lambda = -1$, we say that the body $-\mathscr{B}$ is the *opposite* of $\mathscr{B}$. Moreover, the *Minkowski difference* between the bodies $\mathscr{B}_1$ and $\mathscr{B}_2$ is defined as the sum of $\mathscr{B}_1$ and the opposite of $\mathscr{B}_2$:

$$\mathscr{B}_1 - \mathscr{B}_2 := \mathscr{B}_1 + (-\mathscr{B}_2).$$

More generally, let $\mathscr{B}_1, \ldots, \mathscr{B}_n$ be n bodies of $\mathscr{K}$ and $\lambda_1, \ldots, \lambda_n$ n non-negative scalars. The body

$$\mathscr{B} = \lambda_1\mathscr{B}_1 + \cdots + \lambda_n\mathscr{B}_n \quad \text{(A3)}$$

is the *linear combination* of $\mathscr{B}_1, \ldots, \mathscr{B}_n$ with coefficients $\lambda_1, \ldots, \lambda_n$. Relative to a given origin $o \in \mathscr{E}$, the points $p \in \mathscr{B}$ are described by the linear combinations

$$p - o = \lambda_1(p_1 - o) + \cdots + \lambda_n(p_n - o)$$

as each p_i ranges in $\mathscr{B}_i$, for $i = 1, \ldots, n$. It is easily seen that changing o into o' makes $\mathscr{B}$ in (A3) translate by the vector $(\lambda_1 + \cdots + \lambda_n - 1)(o - o')$, so that, in particular, when $\lambda_1 + \cdots + \lambda_n = 1$ [and the linear combination in (A3) is said to be *convex*], the body $\mathscr{B}$ remains unchanged by the change of origin. In general, the linear combination of bodies of $\mathscr{K}$ delivers a body in $\mathscr{K}$, and so $\mathscr{K}$ is closed under such an algebraic operation.[10]

We denote by $\mathbb{B}^3$ the unit ball in $\mathscr{E}$ with center in the prescribed origin o and by $\mathbb{S}^2 := \partial\mathbb{B}^3$ the unit sphere in $\mathscr{E}$. Let $\mathscr{B} \in \mathscr{K}$ be a convex body. For any $r \geqq 0$, we call $\mathscr{B}_r := \mathscr{B} + r\mathbb{B}^3$ the *parallel body* of $\mathscr{B}$ at the distance r. It can be obtained by the superposition of all balls with radius r whose centers are points of $\mathscr{B}$. Equivalently, $\mathscr{B}_r$ is the body whose points are at Euclidean distances less than or equal to r from (at least) a point of $\mathscr{B}$. Often, for short, we shall also call $\mathscr{B}_r$ the *spherobody* of $\mathscr{B}$ with radius r. For $\mathscr{B} \in \mathscr{K}$, the body $\mathscr{B}_r$ is also a body of $\mathscr{K}$; intuitively, it can be seen as $\mathscr{B}$ thickened by the deposition of a uniform crust of thickness r on its boundary.

In $\mathscr{K}$ we can also introduce a distance that turns it into a *metric space*. To this end we define the *deviation* between two convex bodies.[11] More specifically, let $\mathscr{B}_1$ and $\mathscr{B}_2$ be any two bodies of $\mathscr{K}$ and let $\delta > 0$ be such that $\mathscr{B}_1 \subset \mathscr{B}_2 + \delta\mathbb{B}^3$ and $\mathscr{B}_2 \subset \mathscr{B}_1 + \delta\mathbb{B}^3$. Then we say that the deviation between $\mathscr{B}_1$ and $\mathscr{B}_2$ is less than δ. The greatest lower bound of the deviations between $\mathscr{B}_1$ and $\mathscr{B}_2$ is called the *distance* $d(\mathscr{B}_1, \mathscr{B}_2)$ between $\mathscr{B}_1$ and $\mathscr{B}_2$. Formally,

$$d(\mathscr{B}_1, \mathscr{B}_2) := \liminf\{\delta > 0 | \mathscr{B}_1 \subset \mathscr{B}_2 + \delta\mathbb{B}^3, \mathscr{B}_2 \subset \mathscr{B}_1 + \delta\mathbb{B}^3\}.$$

The function $d : \mathscr{K} \times \mathscr{K} \to \mathbb{R}$ is non-negative and symmetric, and it satisfies the triangle inequality,

$$d(\mathscr{B}_1, \mathscr{B}_3) \leqq d(\mathscr{B}_1, \mathscr{B}_2) + d(\mathscr{B}_2, \mathscr{B}_3),$$

for all bodies $\mathscr{B}_1$, $\mathscr{B}_2$, and $\mathscr{B}_3$ in $\mathscr{K}$. This distance in $\mathscr{K}$ is also called the *Hausdorff distance* and the metric it induces is the *Hausdorff metric* [37] (p. 48).

The distance just introduced in $\mathscr{K}$ makes it possible to define crucial analytical notions such as convergence and approximation. Here we recall only some theorems related to these notions, the ones that are especially relevant to our purposes. We say that a sequence $\{\mathscr{B}_n\}_{n\in\mathbb{N}}$ of bodies of $\mathscr{K}$ converges to $\mathscr{B} \in \mathscr{K}$, whenever $\lim_{n\to\infty} d(\mathscr{B}_n, \mathscr{B}) = 0$. A celebrated theorem by Blaschke, called the *selection theorem*, says that a subsequence can always be selected from an infinite, uniformly bounded set of convex bodies that converges to a convex body [35] (p. 38). This proves that $\mathscr{K}$ is a (sequentially) compact space [42] (p. 160).

Let $\Phi : \mathscr{K} \to \mathbb{R}$ be a functional on $\mathscr{K}$. We say that Φ is *continuous* whenever

$$\lim_{n\to\infty} \Phi(\mathscr{B}_n) = \Phi(\mathscr{B}),$$

for all sequences $\{\mathscr{B}_n\}_{n\in\mathbb{N}}$ of bodies $\mathscr{B}_n \in \mathscr{K}$ converging to $\mathscr{B}$. Notable examples of continuous functionals are the volume $V[\mathscr{B}]$ and the surface area $S[\mathscr{B}]$ of a convex body $\mathscr{B}$. The definition of $V[\mathscr{B}]$ was given by Minkowski [43] (pp. 46–72) [see also [35] (p. 42)] through a limiting process, which also establishes the continuity of V in $\mathscr{K}$. The surface area $S[\mathscr{B}]$ can be defined as the continuous extension of the surface area of convex polyhedra, as these latter can approximate any convex body in the Hausdorff metric [35] (p. 51). Since the functional S is continuous on convex polyhedra, it is so on the whole of $\mathscr{K}$ by its very definition.[12] It was also shown by

[10] These general concepts were introduced by Minkowski [19], although anticipations were also present in the works of both Steiner and Brunn [35] (p. 33).

[11] See, for example, [35] (p. 38).

[12] It is worth remembering that the continuity in the Hausdorff metric of the surface area S is valid only for convex bodies. A well-known example due to Schwarz [and called the *Schwarz lantern* by the resemblance it bears to Chinese paper lanterns [39] (Sec. 3.13)] shows that if the approximating bodies are not convex, their limiting surface area may exceed the surface area of the limiting convex body by any

Steiner [35] (p. 52) that

$$S[\mathscr{B}] = \lim_{\delta \to 0^+} \frac{V[\mathscr{B} + \delta \mathbb{B}^3] - V[\mathscr{B}]}{\delta}, \tag{A4}$$

for all $\mathscr{B} \in \mathscr{K}$.[13] This formula will be encountered again below. Moreover, Minkowski addition defined in (A1) above is continuous in each of its arguments.

A bounded convex body $\mathscr{B}$ can be approximated in the Hausdorff metric by special convex bodies. Several approximation theorems are known to this effect [see, for example, [35] (Sec. 26) and [37] (Sec. 3.3)]. Here we are especially interested in approximating a bounded convex body with convex bodies bounded by smooth surfaces of class at least C^2 with strictly positive principal curvatures; these bodies are in particular strictly convex. This possibility follows from a more general theorem of Minkowski [19] (Sec. 2) [see also [35] (p. 39)], which says that for each convex body $\mathscr{B}$ there is a sequence $\{\mathscr{B}_n\}_{n\in\mathbb{N}}$ of convex bodies such that for each n there is an analytic function $\Omega_n : \mathscr{E} \to \mathbb{R}$ for which

$$p \in \mathscr{B}_n \Leftrightarrow \Omega_n < 1$$

and for every $p \in \partial\mathscr{B}_n$ the tangent plane to $\partial\mathscr{B}_n$ exists and has there a contact of exactly the *first order* with $\mathscr{B}_n$. The class of such smooth bodies with positive curvatures will be denoted by $\mathscr{K}^+$. The theorem just recalled then simply states that $\mathscr{K}^+$ is dense in $\mathscr{K}$. As shown shortly below, this theorem will allow us to extend by continuity to all bodies of $\mathscr{K}$ the *total mean curvature*, a functional properly defined only for bodies in $\mathscr{K}^+$.

2. Total mean curvature

A body $\mathscr{B}$ of $\mathscr{K}^+$ can be represented as the region of $\mathscr{E}$ enclosed by the surface

$$\partial\mathscr{B} = \{p \in \mathscr{E} \,|\, p - o = \boldsymbol{r}(\boldsymbol{v})\}, \tag{A5}$$

where o is a given point of $\mathscr{E}$ and $\boldsymbol{r} : \mathbb{S}^2 \to \mathscr{V}$ is a smooth mapping, which assigns to the unit vector $\boldsymbol{v}$ the vector that brings o into the point of $\partial\mathscr{B}$ where $\boldsymbol{v}$ is the outward unit normal to $\partial\mathscr{B}$ (see Fig. 14, where for convenience the unit sphere $\mathbb{S}^2$ is depicted with origin at o). We call $\boldsymbol{r}$ the *radial* mapping of $\mathscr{B}$.

The outward unit normal to $\partial\mathscr{B}$ can also be regarded as a unit vector field $\boldsymbol{n}$ on $\partial\mathscr{B}$, which by (A5) must satisfy the identity

$$\boldsymbol{v} = \boldsymbol{n}[o + \boldsymbol{r}(\boldsymbol{v})] = \boldsymbol{n}(p) \quad \forall\, \boldsymbol{v} \in \mathbb{S}^2. \tag{A6}$$

As a mapping on $\partial\mathscr{B}$, the field $\boldsymbol{n}$ has a surface gradient $\nabla_s \boldsymbol{n}$, which can be represented as

$$\nabla_s \boldsymbol{n} = \sigma_1 \boldsymbol{e}_1 \otimes \boldsymbol{e}_1 + \sigma_2 \boldsymbol{e}_2 \otimes \boldsymbol{e}_2, \tag{A7}$$

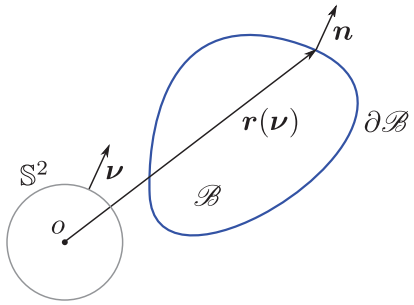

FIG. 14. (Color online) Sketch that describes how the radial mapping $\boldsymbol{r}$ assigns to a unit vector $\boldsymbol{v}$ of $\mathbb{S}^2$ the translation that brings o to the point on $\partial\mathscr{B}$ where $\boldsymbol{v}$ is the unit outward normal to $\partial\mathscr{B}$. The existence of such a mapping is guaranteed by the assumption that $\mathscr{B}$ belongs to $\mathscr{K}^+$.

where the *positive* scalars σ_1 and σ_2 are the principal *curvatures* of $\partial\mathscr{B}$, and the unit vectors $\boldsymbol{e}_1$ and $\boldsymbol{e}_2$ designate the corresponding principal directions of curvature; $\boldsymbol{e}_1$ and $\boldsymbol{e}_2$ are orthogonal to one another and both lie in the plane orthogonal to $\boldsymbol{n}$ (and $\boldsymbol{v}$). The tensor $\nabla_s \boldsymbol{n}$ is also called the *curvature* tensor. The *mean* curvature H and the *Gaussian* curvature K are defined on $\partial\mathscr{B}$ as

$$H := \tfrac{1}{2}(\sigma_1 + \sigma_2) \quad \text{and} \quad K := \sigma_1\sigma_2. \tag{A8}$$

By (A7), we can also write

$$H = \tfrac{1}{2} \operatorname{tr} \nabla_s \boldsymbol{n} = \tfrac{1}{2} \operatorname{div}_s \boldsymbol{n}, \tag{A9}$$

where tr denotes the trace and div_s denotes the surface divergence. For a body $\mathscr{B}$ of $\mathscr{K}^+$ the *total mean curvature* is the functional M defined as

$$M[\mathscr{B}] := \int_{\partial\mathscr{B}} H da(\boldsymbol{n}) = \frac{1}{2} \int_{\partial\mathscr{B}} \operatorname{div}_s \boldsymbol{n} da(\boldsymbol{n}), \tag{A10}$$

where $a(\boldsymbol{n})$ denotes the area measure over $\partial\mathscr{B}$ (where the outer unit normal is the field $\boldsymbol{n}$).

For any second-rank tensor $\mathbf{A}$, the *adjugate* tensor $\mathbf{A}^*$ is characterized by the property that

$$\mathbf{A}^*(\boldsymbol{u} \times \boldsymbol{v}) = \mathbf{A}\boldsymbol{u} \times \mathbf{A}\boldsymbol{v} \quad \forall\, \boldsymbol{u}, \boldsymbol{v} \in \mathscr{V},$$

where $\times$ denotes the cross product in $\mathscr{V}$. It can be shown that[14]

$$\mathbf{A}^* = \left[\mathbf{A}^2 - (\operatorname{tr}\mathbf{A})\mathbf{A} + \tfrac{1}{2}[(\operatorname{tr}\mathbf{A})^2 - \operatorname{tr}\mathbf{A}^2]\mathbf{I}\right]^{\mathsf{T}}, \tag{A11}$$

where $^{\mathsf{T}}$ denotes transposition and $\mathbf{I}$ is the identity tensor. By applying (A11) to $\nabla_s \boldsymbol{n}$ in (A7), we easily see that

$$(\nabla_s \boldsymbol{n})^* = K\boldsymbol{n} \otimes \boldsymbol{n} = K\boldsymbol{v} \otimes \boldsymbol{v}, \tag{A12}$$

where the identity (A6) has been used to write the second equation. The same identity also shows that

$$\nabla_s \boldsymbol{n} \nabla_s \boldsymbol{r} = \mathbf{P}, \tag{A13}$$

where $\mathbf{P} := \mathbf{I} - \boldsymbol{v} \otimes \boldsymbol{v}$ is the orthogonal projection onto the plane orthogonal to $\boldsymbol{v}$ on $\mathbb{S}^2$ and $\nabla_s \boldsymbol{r}$ denotes the surface gradient of $\boldsymbol{r}$ on $\mathbb{S}^2$.

It follows from (A7) and (A13) that

$$\nabla_s \boldsymbol{r} = \rho_1 \boldsymbol{e}_1 \otimes \boldsymbol{e}_1 + \rho_2 \boldsymbol{e}_2 \otimes \boldsymbol{e}_2, \tag{A14}$$

fixed amount. Thus, the Hausdorff topology is only appropriate to describe geometric approximation in $\mathscr{K}$.

[13] Actually, (A4) was the *definition* of surface area adopted by Minkowski for all bodies of $\mathscr{K}$. In $\mathscr{K}$ it agrees with the limiting surface area on approximating polyhedra. The connection between this and other concepts of surface area for nonconvex bodies was explored in [44]; here we shall be contented with defining S only in $\mathscr{K}$.

[14] See also [41] (Sec. 2.11).

where

$$\rho_1 := \frac{1}{\sigma_1} \quad \text{and} \quad \rho_2 := \frac{1}{\sigma_2} \tag{A15}$$

are the principal *radii* of curvature of $\partial\mathscr{B}$. In complete analogy with (A12), we obtain from (A14) and (A15) that

$$(\nabla_{\mathrm{s}}\boldsymbol{r})^* = \frac{1}{K}\boldsymbol{\nu}\otimes\boldsymbol{\nu}, \tag{A16}$$

which allows us to write the surface area dilation ratio[15] for the mapping $\boldsymbol{r}$ that sends $\mathbb{S}^2$ onto $\partial\mathscr{B}$ as

$$\frac{da(\boldsymbol{n})}{da(\boldsymbol{\nu})} = |(\nabla_{\mathrm{s}}\boldsymbol{r})^*\boldsymbol{\nu}| = \frac{1}{K}. \tag{A17}$$

Moreover, it follows from (A14), (A15), (A9), and (A8) that

$$\operatorname{div}_{\mathrm{s}}\boldsymbol{r} = \rho_1+\rho_2 = \frac{\sigma_1+\sigma_2}{\sigma_1\sigma_2} = \frac{1}{K}\operatorname{div}_{\mathrm{s}}\boldsymbol{n}. \tag{A18}$$

The surface-divergence theorem[16] says that

$$\begin{aligned}\int_{\mathscr{S}} \operatorname{div}_{\mathrm{s}}\boldsymbol{u}\, da(\boldsymbol{n}_{\mathscr{S}}) &= \int_{\mathscr{S}} (\operatorname{div}_{\mathrm{s}}\boldsymbol{n}_{\mathscr{S}})\boldsymbol{u}\cdot\boldsymbol{n} da(\boldsymbol{n}_{\mathscr{S}})\\ &= 2\int_{\mathscr{S}} H_{\mathscr{S}}\boldsymbol{u}\cdot\boldsymbol{n} da(\boldsymbol{n}_{\mathscr{S}})\end{aligned} \tag{A19}$$

for any continuously differentiable field $\boldsymbol{u}$ defined on a closed smooth surface $\mathscr{S}$ with outer unit normal $\boldsymbol{n}_{\mathscr{S}}$ and mean curvature $H_{\mathscr{S}}$. By applying (A19) to the case where $\mathscr{S}$ is $\mathbb{S}^2$ and $\boldsymbol{u}=\boldsymbol{r}$, since then $H_{\mathscr{S}}=1$, we see that

$$\int_{\mathbb{S}^2} \operatorname{div}_{\mathrm{s}}\boldsymbol{r}\, da(\boldsymbol{\nu}) = 2\int_{\mathbb{S}^2} \boldsymbol{r}\cdot\boldsymbol{\nu} da(\boldsymbol{\nu}). \tag{A20}$$

By combining (A17), (A18), and (A20), we convert the definition (A10) for M into the following equivalent form:

$$M[\mathscr{B}] = \int_{\mathbb{S}^2} \boldsymbol{r}\cdot\boldsymbol{\nu} da(\boldsymbol{\nu}). \tag{A21}$$

In particular, it follows from (A21) that for $\mathscr{B}$ a ball of radius r, for which $\boldsymbol{r}=r\boldsymbol{\nu}$,

$$M[r\mathbb{B}^3] = 4\pi r. \tag{A22}$$

For this reason, $\frac{1}{4\pi}M[\mathscr{B}]$ is often also called the *mean half-width* of $\mathscr{B}$.[17] Equation (A18), combined with (A17), also lead us to an alternative expression for M,

$$\int_{\mathbb{S}^2} (\rho_1+\rho_2)\, da(\boldsymbol{\nu}) = 2M[\mathscr{B}], \tag{A23}$$

which is often convenient.

Formula (A21) is especially expedient to show how M changes under Minkowski addition in $\mathscr{K}^+$. Let $\boldsymbol{r}_1$ and $\boldsymbol{r}_2$ be the radial mappings for the bodies $\mathscr{B}_1$ and $\mathscr{B}_2$ of $\mathscr{K}^+$ and let $\mathscr{B}_1+\mathscr{B}_2$ be their Minkowski sum. By (A1), the radial mapping $\boldsymbol{r}_{12}$ of $\mathscr{B}_1+\mathscr{B}_2$ is easily seen to be given by

$$\boldsymbol{r}_{12} = \boldsymbol{r}_1+\boldsymbol{r}_2. \tag{A24}$$

[15] See also [41] (Sec. 8.2).
[16] See also [34] (Sec. 5.2.3).
[17] See, for example, [20].

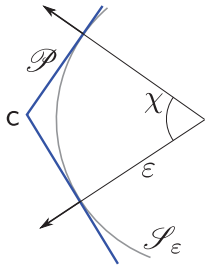

FIG. 15. (Color online) Cross section of a circular cylindrical sector of radius ε rounding the edge of a polyhedron $\mathscr{P}$ running orthogonally to the plane of the drawing through the point C. The angle between the outer unit normals to the adjacent faces of $\mathscr{P}$ is χ.

By (A21) and (A24), we then prove that M is Minkowski additive:

$$M[\mathscr{B}_1+\mathscr{B}_2] = M[\mathscr{B}_1]+M[\mathscr{B}_2], \quad \forall\, \mathscr{B}_1,\mathscr{B}_2\in\mathscr{K}^+. \tag{A25}$$

Suppose, in particular, that $\mathscr{B}_1=\mathscr{B}\in\mathscr{K}^+$ and $\mathscr{B}_2=r\mathbb{B}^3$, so that $\mathscr{B}_1+\mathscr{B}_2=\mathscr{B}_r$, the parallel body of $\mathscr{B}$ at the distance r. By (A25) and (A22),

$$M[\mathscr{B}_r] = M[\mathscr{B}]+4\pi r. \tag{A26}$$

An easy generalization of (A25) follows from remarking that if the bodies $\mathscr{B}_1,\dots,\mathscr{B}_n$ in (A3) are assumed in $\mathscr{K}^+$ and their radial mappings are denoted by $\boldsymbol{r}_1,\dots,\boldsymbol{r}_n$, respectively, then the radial mapping $\boldsymbol{r}$ of the body $\mathscr{B}$ in (A3) is simply $\boldsymbol{r}=\sum_{i=1}^n \lambda_i\boldsymbol{r}_i$. Thus, by (A21), we obtain that

$$M\left[\sum_{i=1}^n \lambda_i\mathscr{B}_i\right] = \sum_{i=1}^n \lambda_i M[\mathscr{B}_i], \quad \forall\, \mathscr{B}_i\in\mathscr{K}^+, \quad \lambda_i\geqq 0. \tag{A27}$$

In particular, for a scalar multiple of a single body $\mathscr{B}\in\mathscr{K}^+$, (A27) becomes

$$M[\lambda\mathscr{B}] = \lambda M[\mathscr{B}]. \tag{A28}$$

The definition of M can be extended to all bodies of $\mathscr{K}$ by continuity.[18] Here we see some elementary examples, particularly significant to our development in the main body of the paper [see also [45] (Sec. III.13.8) and the whole classical book [36], devoted to three-dimensional convex bodies]. When a sequence of bodies $\{\mathscr{B}_n\}_{n\in\mathbb{N}}$ in $\mathscr{K}^+$ approximate a polyhedron $\mathscr{P}$, it is clear from (A10) that the boundaries of $\mathscr{B}_n$ that approximate flat faces of $\mathscr{P}$ will eventually contribute nothing to $M[\mathscr{P}]$ as $n\to\infty$. The edges of $\mathscr{P}$, however, capture a positive contribution. This can be seen by regarding a single edge of length L common to two faces of $\mathscr{P}$ with outer unit normals making the angle χ as approached by a circular cylindrical surface $\mathscr{S}_\varepsilon$ of length L, radius ε, and angular amplitude χ (see Fig. 15).

[18] And so do also Eqs. (A27) and (A28).

Since for $\mathscr{S}_\varepsilon$, $\sigma_1 = 0$ and $\sigma_2 = \frac{1}{\varepsilon}$, the contribution of $\mathscr{S}_\varepsilon$ to M is

$$M_{\mathscr{S}_\varepsilon} = \frac{1}{2\varepsilon}\varepsilon\chi L = \frac{1}{2}L\chi, \tag{A29}$$

and we conclude that for a polyhedron $\mathscr{P}$ with N edges,

$$M[\mathscr{P}] = \frac{1}{2}\sum_{i=1}^{N} L_i\chi_i, \tag{A30}$$

where the sum is extended to all edges, each with length L_i and outer normals' angle χ_i. In particular, for a parallelepiped $\mathscr{P}$ whose concurrent edges have length L_1, L_2, and L_3, (A30) delivers

$$M[\mathscr{P}] = \pi(L_1 + L_2 + L_3).$$

Likewise, if $\mathscr{B}$ possesses a curved edge of length L, along which the limiting outer unit normals to $\partial\mathscr{B}$ make the angle $\chi(s)$, where s is the arc length along a parametrization of the edge, it will contribute to $M[\mathscr{B}]$ the quantity

$$M_e = \frac{1}{2}\int_0^L \chi(s)ds,$$

which results from a limit similar (but not identical) to the one in (A29).

With the aid of (A2), we can compute M for a circular *cylinder* $\mathscr{C}$ of height L and radius R. Since the mean curvature of the lateral surface of $\mathscr{C}$ is $H = \frac{1}{2R}$ and the normals' angle is $\chi = \frac{\pi}{2}$ for both edges (each of length $2\pi R$), from (A2) we readily obtain that

$$M[\mathscr{C}] = \pi(L + \pi R). \tag{A31}$$

In particular, it follows from setting $R = 0$ in (A31) that for a *rod* $\mathscr{R}$ of length L,

$$M[\mathscr{R}] = \pi L. \tag{A32}$$

Similarly, it follows from setting $L = 0$ in (A31) that for a *disk* $\mathscr{D}$ of radius R,

$$M[\mathscr{D}] = \pi^2 R. \tag{A33}$$

Both these limiting values of $M[\mathscr{C}]$ will be recalled below.

Finally, we compute M for a circular cone $\mathscr{C}^\alpha$ with slant height L and semiamplitude α. The radius R and the height h of $\mathscr{C}^\alpha$ are given by

$$R = L\sin\alpha \quad \text{and} \quad h = L\cos\alpha, \tag{A34}$$

respectively (see Fig. 16).

First, the vertex v does not contribute to M, as is easily seen by remarking that on a spherical cap $\mathscr{S}_\varepsilon$ of radius ε approximating v, M would scale linearly with ε in the limit as $\varepsilon \to 0$, since $H = \frac{1}{\varepsilon}$ for $\mathscr{S}_\varepsilon$, while the area of $\mathscr{S}_\varepsilon$ is proportional to ε^2. Second, in cylindrical coordinates (r,ϑ,z), the outer unit normal $\boldsymbol{n}$ to the lateral surface of $\mathscr{C}^\alpha$ can be written as

$$\boldsymbol{n} = \sin\alpha\,\boldsymbol{e}_z + \cos\alpha\,\boldsymbol{e}_r,$$

so that

$$\nabla_s\boldsymbol{n} = \frac{\cos\alpha}{r(s)}\boldsymbol{e}_\vartheta \otimes \boldsymbol{e}_\vartheta,$$

where

$$r(s) = s\sin\alpha \quad \text{and} \quad a(s) = s\cos\alpha$$

are the radius and height of the cone with slant height s that runs over $\mathscr{C}^\alpha$ (see Fig. 16). Thus, on the lateral boundary of $\mathscr{C}^\alpha$ the mean curvature is delivered by the following function of s:

$$H = \frac{\cot\alpha}{2s},$$

and since the normals' angle along the base's rim is $\chi = \frac{\pi}{2} + \alpha$, we arrive at

$$\begin{aligned} M[\mathscr{C}^\alpha] &= \frac{1}{2}2\pi R\left(\frac{\pi}{2} + \alpha\right) + \int_0^L 2\pi r(s)\frac{\cot\alpha}{2s}ds \\ &= \pi L\left[\left(\frac{\pi}{2} + \alpha\right)\sin\alpha + \cos\alpha\right], \end{aligned} \tag{A35}$$

where use has also been made of (A34).

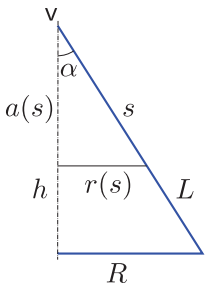

FIG. 16. (Color online) Cross section of a circular cone with height h and radius R, which are related to the slant height L and the semiamplitude α through (A34). The arc-length parameter s, which ranges in $[0,L]$, describes a generatrix from the vertex v to the base. Correspondingly, $r(s)$ and $a(s)$ are the radius and height of the cone with slant height s.

3. Surface area

In addition to Minkowski's definition (A4), the surface area $S[\mathscr{B}]$ of a convex body $\mathscr{B} \in \mathscr{K}^+$ can also be expressed through the formula

$$\begin{aligned} S[\mathscr{B}] &= \int_{\partial\mathscr{B}} da(\boldsymbol{n}) = \int_{\mathbb{S}^2}\frac{1}{K}da(\boldsymbol{v}) \\ &= \int_{\mathbb{S}^2}\boldsymbol{v}\cdot(\nabla_s\boldsymbol{r})^*\boldsymbol{v}da(\boldsymbol{v}), \end{aligned} \tag{A36}$$

where both (A18) and (A17) have also been employed. An alternative expression for S is often useful; it is obtained with

the aid of (A18) and (A19) as follows:

$$\int_{\mathbb{S}^2} (\boldsymbol{\nu}\cdot\boldsymbol{r})\,(\rho_1+\rho_2)\,da(\boldsymbol{\nu}) = \int_{\partial\mathscr{B}} \boldsymbol{n}\cdot(p-o)\,\mathrm{div}_{\mathrm{s}}\,\boldsymbol{n}\,da(\boldsymbol{n}) = \int_{\partial\mathscr{B}} \mathrm{div}_{\mathrm{s}}(p-o)\,da(\boldsymbol{n}) = 2S[\mathscr{B}], \tag{A37}$$

where we have also used (A18) and the fact that $\mathrm{div}_{\mathrm{s}}(p-o) = \mathrm{tr}\,\nabla_{\mathrm{s}}(p-o) = \mathrm{tr}\,\mathbf{P} = 2$.

It follows from (A24) and (A36) that the body $\mathscr{B}_1+\mathscr{B}_2$ has surface area

$$S[\mathscr{B}_1+\mathscr{B}_2] = \int_{\mathbb{S}^2} \boldsymbol{\nu}\cdot(\nabla_{\mathrm{s}}\boldsymbol{r}_1+\nabla_{\mathrm{s}}\boldsymbol{r}_2)^*\boldsymbol{\nu}\,da(\boldsymbol{\nu}), \tag{A38}$$

since $\nabla_{\mathrm{s}}\boldsymbol{r}_{12} = \nabla_{\mathrm{s}}\boldsymbol{r}_1+\nabla_{\mathrm{s}}\boldsymbol{r}_2$. By (A11), we easily see that[19]

$$(\mathbf{A}+\mathbf{B})^* = \mathbf{A}^*+\mathbf{B}^*+\mathbf{A}^{\mathsf{T}}\mathbf{B}^{\mathsf{T}}+\mathbf{B}^{\mathsf{T}}\mathbf{A}^{\mathsf{T}}-(\mathrm{tr}\,\mathbf{A})\mathbf{B}^{\mathsf{T}}-(\mathrm{tr}\,\mathbf{B})\mathbf{A}^{\mathsf{T}} + [(\mathrm{tr}\,\mathbf{A})(\mathrm{tr}\,\mathbf{B})-\mathrm{tr}(\mathbf{AB})]\mathbf{I}, \tag{A39}$$

for $\mathbf{A}$ and $\mathbf{B}$ any two second-rank tensors. By applying (A14) to $\boldsymbol{r}_1$ and $\boldsymbol{r}_2$, we can write

$$\nabla_{\mathrm{s}}\boldsymbol{r}_i = \rho_1^{(i)}\boldsymbol{e}_1^{(i)}\otimes\boldsymbol{e}_1^{(i)}+\rho_2^{(i)}\boldsymbol{e}_2^{(i)}\otimes\boldsymbol{e}_2^{(i)}, \quad i=1,2, \tag{A40}$$

which shows that both $\nabla_{\mathrm{s}}\boldsymbol{r}_1$ and $\nabla_{\mathrm{s}}\boldsymbol{r}_2$ are symmetric tensors that annihilate the normal $\boldsymbol{\nu}$. From (A38) and (A39), we then obtain that

$$S[\mathscr{B}_1+\mathscr{B}_2] = S[\mathscr{B}_1]+S[\mathscr{B}_2]+\int_{\mathbb{S}^2}[(\mathrm{tr}\,\nabla_{\mathrm{s}}\boldsymbol{r}_1)(\mathrm{tr}\,\nabla_{\mathrm{s}}\boldsymbol{r}_2) - \mathrm{tr}(\nabla_{\mathrm{s}}\boldsymbol{r}_1\nabla_{\mathrm{s}}\boldsymbol{r}_2)]da(\boldsymbol{\nu}). \tag{A41}$$

For any given $\boldsymbol{\nu}\in\mathbb{S}^2$, both unit vector pairs $(\boldsymbol{e}_1^{(1)},\boldsymbol{e}_2^{(1)})$ and $(\boldsymbol{e}_1^{(2)},\boldsymbol{e}_2^{(2)})$ lie in the plane orthogonal to $\boldsymbol{\nu}$, and so there is an angle $\vartheta\in[0,\pi]$, depending on $\boldsymbol{\nu}$, such that

$$\boldsymbol{e}_1^{(2)}\otimes\boldsymbol{e}_1^{(2)} = \cos^2\vartheta\,\boldsymbol{e}_1^{(1)}\otimes\boldsymbol{e}_1^{(1)}+\sin^2\vartheta\,\boldsymbol{e}_2^{(1)}\otimes\boldsymbol{e}_2^{(1)} + \cos\vartheta\sin\vartheta\left(\boldsymbol{e}_1^{(1)}\otimes\boldsymbol{e}_2^{(1)}+\boldsymbol{e}_2^{(1)}\otimes\boldsymbol{e}_1^{(1)}\right), \tag{A42a}$$

$$\boldsymbol{e}_2^{(2)}\otimes\boldsymbol{e}_2^{(2)} = \sin^2\vartheta\,\boldsymbol{e}_1^{(1)}\otimes\boldsymbol{e}_1^{(1)}+\cos^2\vartheta\,\boldsymbol{e}_2^{(1)}\otimes\boldsymbol{e}_2^{(1)} - \cos\vartheta\sin\vartheta\left(\boldsymbol{e}_1^{(1)}\otimes\boldsymbol{e}_2^{(1)}+\boldsymbol{e}_2^{(1)}\otimes\boldsymbol{e}_1^{(1)}\right). \tag{A42b}$$

Making use of (A42), we readily give (A41) the following form:

$$S[\mathscr{B}_1+\mathscr{B}_2] = S[\mathscr{B}_1]+S[\mathscr{B}_2] + \int_{\mathbb{S}^2}\Big[\sin^2\vartheta\left(\rho_1^{(1)}\rho_1^{(2)}+\rho_2^{(1)}\rho_2^{(2)}\right) + \cos^2\vartheta\left(\rho_1^{(1)}\rho_2^{(2)}+\rho_2^{(1)}\rho_1^{(2)}\right)\Big]da(\boldsymbol{\nu}). \tag{A43}$$

A special instance of (A43) is easily computable, that is, when $\mathscr{B}_1$ is any body $\mathscr{B}$ in $\mathscr{K}^+$ and $\mathscr{B}_2$ is a ball of radius r, so that $\rho_1^{(2)} = \rho_2^{(2)} = r$. In this case $\mathscr{B}_1+\mathscr{B}_2 = \mathscr{B}_r$, and we have

$$S[\mathscr{B}_r] = S[\mathscr{B}]+4\pi r^2+r\int_{\mathbb{S}^2}(\rho_1+\rho_2)da(\boldsymbol{\nu}) = S[\mathscr{B}]+4\pi r^2+2rM[\mathscr{B}], \tag{A44}$$

where (A23) has also been used. This formula for the surface area of a spherobody has been proved in $\mathscr{K}^+$; since both M and S are continuous functionals, the validity of (A44) can be extended to all convex bodies. A similar formula will be given below for the volume.

More generally, if both bodies $\mathscr{B}_1$ and $\mathscr{B}_2$ have principal radii of curvature bounded in the interval $[\rho_{\mathrm{m}},\rho_{\mathrm{M}}]$, then (A43) implies the inequalities

$$8\pi\rho_{\mathrm{m}}^2 \leqq S[\mathscr{B}_1+\mathscr{B}_2]-S[\mathscr{B}_1]-S[\mathscr{B}_2] \leqq 8\pi\rho_{\mathrm{M}}^2.$$

Finally, by (A11), it follows from (A36) that

$$S[\lambda\mathscr{B}] = \lambda^2 S[\mathscr{B}]. \tag{A45}$$

4. Volume

By the classical divergence theorem, the volume $V[\mathscr{B}]$ of a convex body $\mathscr{B}\in\mathscr{K}^+$ is also delivered by the surface integral,

$$V[\mathscr{B}] = \frac{1}{3}\int_{\partial\mathscr{B}}\boldsymbol{n}\cdot(p-o)da(\boldsymbol{n}),$$

which, by (A17) and (A16), can also be given the equivalent forms

$$V[\mathscr{B}] = \frac{1}{3}\int_{\mathbb{S}^2}(\boldsymbol{\nu}\cdot\boldsymbol{r})\frac{1}{K}da(\boldsymbol{\nu}) \tag{A46a}$$

$$= \frac{1}{3}\int_{\mathbb{S}^2}(\boldsymbol{\nu}\cdot\boldsymbol{r})\boldsymbol{\nu}\cdot(\nabla_{\mathrm{s}}\boldsymbol{r})^*\boldsymbol{\nu}\,da(\boldsymbol{\nu}). \tag{A46b}$$

For any body $\mathscr{B}$, the *centroid* c is the point defined by the property

$$c-o := \frac{1}{V[\mathscr{B}]}\int_{\mathscr{B}}(p-o)dv(p). \tag{A47}$$

For a convex body $\mathscr{B}\in\mathscr{K}^+$, also with the aid of (A16) and (A17), Eq. (A47) can equivalently be expressed in terms of the radial mapping $\boldsymbol{r}$ of $\mathscr{B}$:

$$c-o = \frac{1}{2}\frac{1}{V[\mathscr{B}]}\int_{\partial\mathscr{B}}[(p-o)\otimes(p-o)]\boldsymbol{n}da(\boldsymbol{n}) = \frac{1}{2}\frac{1}{V[\mathscr{B}]}\int_{\mathbb{S}^2}(\boldsymbol{r}\cdot\boldsymbol{\nu})[\boldsymbol{\nu}\cdot(\nabla_{\mathrm{s}}\boldsymbol{r})^*\boldsymbol{\nu}]\boldsymbol{r}da(\boldsymbol{\nu}).$$

It easily follows from (A47) that translating the origin o does not affect c, which is thus uniquely identified by the body $\mathscr{B}$. Moreover, if c_1 is the centroid of the body $\mathscr{B}_1$ and c_2 is the centroid of the body $\mathscr{B}_2$, it follows from (A1) and (A47) that the centroid c of the body $\mathscr{B} = \mathscr{B}_1+\mathscr{B}_2$ is simply given by

$$c-o = (c_1-o)+(c_2-o). \tag{A48}$$

This in particular shows that if the origin o is chosen in the centroid c_1 of $\mathscr{B}_1$, then the centroid c of $\mathscr{B}_1+\mathscr{B}_2$ coincides with the centroid c_2 of $\mathscr{B}_2$, and if both centroids c_1 and c_2 coincide with o, then so also does c.

We now compute the volume $V[\mathscr{B}_1+\mathscr{B}_2]$ of the sum $\mathscr{B}_1+\mathscr{B}_2$ of two bodies in $\mathscr{K}^+$. By letting $\boldsymbol{r} = \boldsymbol{r}_{12}$ in (A46b) and

[19] See also [41] (p. 24).

using (A24), by (A39) and (A40), we easily arrive at

$$V[\mathscr{B}_1+\mathscr{B}_2] = V[\mathscr{B}_1]+V[\mathscr{B}_2] + \frac{1}{3}\int_{\mathbb{S}^2}\left(\boldsymbol{v}\cdot\boldsymbol{r}_1\frac{1}{K^{(2)}}+\boldsymbol{v}\cdot\boldsymbol{r}_2\frac{1}{K^{(1)}}\right)da(\boldsymbol{v}) + \frac{1}{3}\int_{\mathbb{S}^2}(\boldsymbol{v}\cdot\boldsymbol{r}_1+\boldsymbol{v}\cdot\boldsymbol{r}_2) \times\left[\sin^2\vartheta\left(\rho_1^{(1)}\rho_1^{(2)}+\rho_2^{(1)}\rho_2^{(2)}\right) +\cos^2\vartheta\left(\rho_1^{(1)}\rho_2^{(2)}+\rho_2^{(1)}\rho_1^{(2)}\right)\right]da(\boldsymbol{v}), \tag{A49}$$

where $K^{(1)}=(\rho_1^{(1)}\rho_2^{(1)})^{-1}$ and $K^{(2)}=(\rho_1^{(2)}\rho_2^{(2)})^{-1}$ are the Gaussian curvatures of $\partial\mathscr{B}_1$ and $\partial\mathscr{B}_2$, respectively, and use of (A42) has also been made.

A notable application of (A49) is to the volume $V[\mathscr{B}_r]$ of the spherobody $\mathscr{B}_r$ of a body $\mathscr{B}\in\mathscr{K}^+$. This entails taking $\rho_1^{(2)}=\rho_2^{(2)}=r$, which easily changes (A49) into

$$V[\mathscr{B}_r] = V[\mathscr{B}]+\frac{4\pi}{3}r^3+\frac{1}{3}r^2\int_{\mathbb{S}^2}\boldsymbol{v}\cdot\boldsymbol{r}da(\boldsymbol{v}) + \frac{1}{3}r\int_{\mathbb{S}^2}\frac{1}{K}da(\boldsymbol{v})+\frac{1}{3}r^2\int_{\mathbb{S}^2}(\rho_1+\rho_2)da(\boldsymbol{v}) + \frac{1}{3}r\int_{\mathbb{S}^2}(\boldsymbol{v}\cdot\boldsymbol{r})(\rho_1+\rho_2)da(\boldsymbol{v}), \tag{A50}$$

where ρ_1 and ρ_2 are the principal radii of curvature of $\partial\mathscr{B}$. Use of both (A21) and (A36) for M and S and the alternative expressions in (A23) and (A37) transforms (A50) into

$$V[\mathscr{B}_r] = V[\mathscr{B}]+rS[\mathscr{B}]+r^2M[\mathscr{B}]+\frac{4\pi}{3}r^3, \tag{A51}$$

whence, in particular, (A4) follows. Equation (A51), which is a celebrated formula of Steiner, shows how $V[\mathscr{B}_r]$ can be expressed as a polynomial of degree 3 in r. The interested reader is referred to [39] (p. 153) for both a different derivation of this formula and its extensions to higher-dimensional Euclidean spaces.

Finally, the scaling for V that supplements (A28) and (A45) easily follows from (A46b),

$$V[\lambda\mathscr{B}] = \lambda^3 V[\mathscr{B}]. \tag{A52}$$

5. Averages

Despite their apparent simplicity, both formulas (A43) and (A49) are usually hard to compute. In particular, this explains why closed-form expressions for the excluded volume of two bodies, which, by (4) and (7), is indeed a special instance of (A49), are so rarely available, even for convex bodies. However, a consequence can in general be drawn from both (A43) and (A49), which has played an important role in our development in the main body of the paper. This is obtained by assuming $\mathscr{B}_1$ to be given in $\mathscr{K}^+$, while leaving $\mathscr{B}_2$ take all possible orientations in space relative to $\mathscr{B}_1$, that is, subjecting $\mathscr{B}_2$ to all rotations $\mathbf{Q}$ in the special orthogonal group $\mathsf{SO}(3)$. Simple expressions can be obtained from (A43) and (A49) for the surface area $S[\mathscr{B}_1+\mathscr{B}_2]$ and volume $V[\mathscr{B}_1+\mathscr{B}_2]$ averaged over all possible orientations.

Formally, for any given $\mathscr{B}\in\mathscr{K}^+$ and $\mathbf{Q}\in\mathsf{SO}(3)$, we denote by $\mathbf{Q}\{\mathscr{B}\}$ the *rotated* body[20]

$$\mathbf{Q}\{\mathscr{B}\} := \{p^*\in\mathscr{E}\,|\,(p^*-o)=\mathbf{Q}(p-o),\ \forall\ p\in\mathscr{B}\}. \tag{A53}$$

There are several ways to represent $\mathsf{SO}(3)$. One is to regard it as the set $\mathbb{T}:=\mathbb{S}^2\times[0,\pi]$; we represent a rotation $\mathbf{Q}$ through a pair $(\boldsymbol{e},\varphi)$, where $\boldsymbol{e}\in\mathbb{S}^2$ designates an oriented rotation axis and $\varphi\in[0,\pi]$ is a rotation angle. Geometrically, $\mathsf{SO}(3)$ is thus identified with a ball of radius π where points diametrically opposed on the boundary are treated as equivalent. It can be shown [46] (p. 238) [see also [47] (Chap. 8)] that in this representation the *density* of rotations in $\mathbb{T}$ is given by the function $g(\varphi):=\frac{2}{\varphi^2}(1-\cos\varphi)$ and that consequently the total (Haar) measure of $\mathbb{T}$ is $|\mathbb{T}|=8\pi^2$. For any functional F in $\mathscr{K}^+$, we define the *isotropic average*

$$\langle F\rangle[\mathscr{B}] := \langle F[\mathbf{Q}\{\mathscr{B}\}]\rangle_{\mathbf{Q}} := \frac{1}{8\pi^2}\int_{\mathbb{T}}F[\mathbf{Q}(\omega)\{\mathscr{B}\}]\,d\omega, \tag{A54}$$

where ω is a parametrization of $\mathbb{T}$. In particular, in the $(\boldsymbol{e},\varphi)$ parametrization, $d\omega=2(1-\cos\varphi)d\varphi da(\boldsymbol{e})$. Clearly, for a functional F invariant under $\mathsf{SO}(3)$, (A54) reduces to

$$\langle F\rangle[\mathscr{B}] = F[\mathscr{B}],\quad \forall\ \mathscr{B}\in\mathscr{K}^+.$$

For short, we shall also employ the following notation:

$$\langle F\rangle[\mathscr{B}_1,\mathscr{B}_2] := \langle F[\mathscr{B}_1+\mathbf{Q}\{\mathscr{B}_2\}]\rangle_{\mathbf{Q}}. \tag{A55}$$

If F is invariant under $\mathsf{SO}(3)$, since the Minkowski addition is also invariant,

$$\langle F[\mathscr{B}_1+\mathbf{Q}\{\mathscr{B}_2\}]\rangle_{\mathbf{Q}} = \langle F[\mathbf{Q}^{\mathsf{T}}\{\mathscr{B}_1\}+\mathscr{B}_2]\rangle_{\mathbf{Q}^{\mathsf{T}}} = \langle F[\mathscr{B}_2+\mathbf{Q}\{\mathscr{B}_1\}]\rangle_{\mathbf{Q}},$$

which, written in the notation (A55), amounts to the symmetry of $\langle F\rangle[\mathscr{B}_1,\mathscr{B}_2]$ in the bodies $\mathscr{B}_1$ and $\mathscr{B}_2$:

$$\langle F\rangle[\mathscr{B}_1,\mathscr{B}_2] = \langle F\rangle[\mathscr{B}_2,\mathscr{B}_1],\quad \forall\ \mathscr{B}_1,\mathscr{B}_2\in\mathscr{K}^+.$$

For given bodies $\mathscr{B}_1$ and $\mathscr{B}_2$ in $\mathscr{K}^+$, both represented as in (A5), we can take $\omega=(\boldsymbol{v},\vartheta)$, where $\boldsymbol{v}\in\mathbb{S}^2$ is the unit normal common to both $\partial\mathscr{B}_1$ and $\partial\mathscr{B}_2$, and ϑ is the angle defined by (A42). With these identifications, the average defined by (A55) then becomes

$$\langle F\rangle[\mathscr{B}_1,\mathscr{B}_2] = \left\langle\frac{1}{2\pi}\int_0^\pi 2(1-\cos\vartheta)F[\mathscr{B}_1+\mathbf{Q}(\boldsymbol{v},\vartheta)\{\mathscr{B}_2\}]\,d\vartheta\right\rangle_{\boldsymbol{v}}, \tag{A56}$$

where

$$\langle\cdot\rangle_{\boldsymbol{v}} := \frac{1}{4\pi}\int_{\mathbb{S}^2}(\cdot)da(\boldsymbol{v}).$$

By applying (A56) to (A43), since S is an invariant functional, we easily arrive at

$$\langle S\rangle[\mathscr{B}_1,\mathscr{B}_2] = S[\mathscr{B}_1]+S[\mathscr{B}_2] + \frac{1}{2}\langle\rho_1^{(2)}+\rho_2^{(2)}\rangle_{\boldsymbol{v}}\int_{\mathbb{S}^2}(\rho_1^{(1)}+\rho_2^{(1)})da(\boldsymbol{v}),$$

[20] Here the origin o is chosen so as to agree with the one understood in the definition of Minkowski addition in (A1).

which by (A23) yields

$$\langle S\rangle[\mathscr{B}_1,\mathscr{B}_2]=S[\mathscr{B}_1]+S[\mathscr{B}_2]+\frac{1}{2\pi}M[\mathscr{B}_1]M[\mathscr{B}_2]. \quad \text{(A57)}$$

Likewise, by applying (A56) to (A49), we first obtain that

$$\begin{aligned}\langle V\rangle[\mathscr{B}_1,\mathscr{B}_2]&=V[\mathscr{B}_1]+V[\mathscr{B}_2]+\frac{1}{3}\left\langle\frac{1}{K^{(2)}}\right\rangle_{\boldsymbol{\nu}}\int_{\mathbb{S}^2}\boldsymbol{\nu}\cdot\boldsymbol{r}_1 da(\boldsymbol{\nu})\\&+\frac{1}{3}\langle\boldsymbol{\nu}\cdot\boldsymbol{r}_2\rangle_{\boldsymbol{\nu}}\int_{\mathbb{S}^2}\frac{1}{K^{(1)}}da(\boldsymbol{\nu})\\&+\frac{1}{6}\langle\rho_1^{(2)}+\rho_2^{(2)}\rangle_{\boldsymbol{\nu}}\int_{\mathbb{S}^2}\boldsymbol{\nu}\cdot\boldsymbol{r}_1\big(\rho_1^{(1)}+\rho_2^{(1)}\big)da(\boldsymbol{\nu})\\&+\frac{1}{6}\big\langle\boldsymbol{\nu}\cdot\boldsymbol{r}_2\big(\rho_1^{(2)}+\rho_2^{(2)}\big)\big\rangle_{\boldsymbol{\nu}}\int_{\mathbb{S}^2}\big(\rho_1^{(1)}+\rho_2^{(1)}\big)da(\boldsymbol{\nu}),\end{aligned}$$

which, by (A36), (A37), (A21), and (A23) then becomes

$$\begin{aligned}\langle V\rangle[\mathscr{B}_1,\mathscr{B}_2]=V[\mathscr{B}_1]+V[\mathscr{B}_2]+\frac{1}{4\pi}(M[\mathscr{B}_1]S[\mathscr{B}_2]\\+M[\mathscr{B}_2]S[\mathscr{B}_1]).\end{aligned} \quad \text{(A58)}$$

Both formulas (A57) and (A58) are also derived in [48] by use of a different method.[21] Moreover, Kihara [49,50] credits Isihara [51] and Isihara and Hayashida [52,53] for having found (A58), although he seems to be aware that a proof had also been contained in [19].

6. Special spherobodies

In this final section, we collect a catalog of formulas, variously used in the main body of the paper, where the expressions of the functionals M, S, and V for special parallel bodies are recorded, as they follow from a direct application of (A26), (A44), and (A51).

a. Spherorods

A *spherorod* $\mathscr{R}_r$ is the Minkowski sum of a rod $\mathscr{R}$ of length L and the ball $r\mathbb{B}^3$ of radius r. By (A32), since $S[\mathscr{R}]=0$ and $V[\mathscr{R}]=0$, it follows from (A26), (A44), and (A51) that

$$M[\mathscr{R}_r]=4\pi r+\pi L, \quad \text{(A59a)}$$

$$S[\mathscr{R}_r]=4\pi r^2+2\pi rL, \quad \text{(A59b)}$$

$$V[\mathscr{R}_r]=\frac{4\pi}{3}r^3+\pi r^2L. \quad \text{(A59c)}$$

While a spherorod is usually called a *spherocylinder* in the literature, we prefer reserving this latter name for the parallel body of a cylinder, in keeping with our general definition of a spherobody. In doing so, we agree with the suggestion of Mulder [20], who also proposed to call a *true* spherocylinder what here is simply called a spherocylinder.

b. Spherodisks

A *spherodisk* $\mathscr{D}_r$ is the Minkowski sum of a disk $\mathscr{D}$ of radius L and the ball $r\mathbb{B}^3$ of radius r.[22] By (A33), since $S[\mathscr{D}]=2\pi L^2$ (as both faces of $\mathscr{D}$ contribute to its total surface area) and $V[\mathscr{D}]=0$, it follows from (A26), (A44), and (A51) that

$$M[\mathscr{D}_r]=4\pi r+\pi^2L, \quad \text{(A60a)}$$

$$S[\mathscr{D}_r]=4\pi r^2+2\pi^2rL+2\pi L^2, \quad \text{(A60b)}$$

$$V[\mathscr{D}_r]=\frac{4\pi}{3}r^3+\pi^2r^2L+2\pi rL^2. \quad \text{(A60c)}$$

c. Spherocones

A *spherocone* $\mathscr{C}^\alpha_r$ is the Minkowski sum of a cone $\mathscr{C}^\alpha$ with semiamplitude α and slant height L and the ball $r\mathbb{B}^3$ of radius r. By (A35), and since

$$S[\mathscr{C}^\alpha]=\pi L^2\sin\alpha(1+\sin\alpha), \quad \text{(A61a)}$$

$$V[\mathscr{C}^\alpha]=\tfrac{1}{3}\pi L^3\sin^2\alpha\cos\alpha, \quad \text{(A61b)}$$

it follows from (A26), (A44), and (A51) that

$$M\big[\mathscr{C}^\alpha_r\big]=4\pi r+\pi L\left[\left(\frac{\pi}{2}+\alpha\right)\sin\alpha+\cos\alpha\right], \quad \text{(A62a)}$$

$$\begin{aligned}S\big[\mathscr{C}^\alpha_r\big]&=4\pi r^2+2\pi rL\left[\left(\frac{\pi}{2}+\alpha\right)\sin\alpha+\cos\alpha\right]\\&+\pi L^2\sin\alpha(1+\sin\alpha),\end{aligned} \quad \text{(A62b)}$$

$$\begin{aligned}V\big[\mathscr{C}^\alpha_r\big]&=\frac{4\pi}{3}r^3+\pi r^2L\left[\left(\frac{\pi}{2}+\alpha\right)\sin\alpha+\cos\alpha\right]\\&+\pi rL^2\sin\alpha(1+\sin\alpha)+\frac{1}{3}\pi L^3\cos\alpha\sin^2\alpha.\end{aligned} \quad \text{(A62c)}$$

It should be noted that Eqs. (A62) reproduce the corresponding Eqs. (A59) and (A60) for spherorods and spherodisks, by setting $\alpha=0^\circ$ and $\alpha=90^\circ$, respectively. Moreover, (A62) are instrumental in Sec. V to obtain via (A58) the average excluded volume of two identical spherocones.

APPENDIX B: SHAPE-RECONSTRUCTION METHOD

In this Appendix we describe the algorithm adopted for triangulating the boundary $\partial\mathscr{B}_e\{\mathscr{B}_1,\mathscr{B}_2\}$ of the excluded body for any two bodies $\mathscr{B}_1$ and $\mathscr{B}_2$ in the class of *spherocones*, including both *spherorods* and *spherodisks* as limiting cases. The algorithm is organized as a pipeline of two procedures, to be executed synchronously: the first procedure generates a stream of random points from the target surface $\partial\mathscr{B}_e\{\mathscr{B}_1,\mathscr{B}_2\}$ and the second procedure progressively adapts to this stream a purpose-specific, self-organizing network that converges eventually to a complete triangulation of the target surface. In the rest of the Appendix these two procedures are explained in detail.

1. Randomly generated point samples

The stream of random points that is required by the second procedure must provide a complete coverage of the target surface. More precisely, the random points must be generated with positive probability almost everywhere on $\partial\mathscr{B}_e$, i.e., excluding subsets of zero measure only. On the other hand, for reasons to be clarified later, the overall algorithm does not require uniform sampling probability on $\partial\mathscr{B}_e$, although it may converge more slowly in the regions where the probability is

[21] Also called the *convex-body coordinates* method.

[22] Here we denote by L the radius of $\mathscr{D}$ instead of R, as in (A33), to recover $\mathscr{D}_r$ more easily as a limiting spherocone.

lower. The reconstruction procedure, moreover, does not make use of the information about the surface normal at each random point.

Relations (1) and (4) are also the basis for generating random points from $\partial\mathscr{B}_e\{\mathscr{B}_1,\mathscr{B}_2\}$. In particular, when both $\mathscr{B}_1$ and $\mathscr{B}_2$ are in $\mathscr{K}^+$, such random points can be generated through the equation

$$\boldsymbol{r}_{12}(\boldsymbol{v}) = \boldsymbol{r}_1(\boldsymbol{v}) + \boldsymbol{r}_2^*(\boldsymbol{v}), \tag{B1}$$

where $\boldsymbol{v}$ is a random vector with uniform probability on $\mathbb{S}^2$. Note however that, in light of (A38), the probability induced by $\boldsymbol{v}$ on $\partial\mathscr{B}_e$ is inversely proportional to the surface area dilation ratio and it becomes arbitrarily low when the modulus of $[\nabla_s \boldsymbol{r}_{12}(\boldsymbol{v})]^* \boldsymbol{v}$ grows significantly.

This entails that (B1) is not applicable to bodies that are in $\mathscr{K}$ but not in $\mathscr{K}^+$, like spherocones, since their surfaces contain areas of positive measure where K is 0 and so is the probability induced by a uniform random $\boldsymbol{v}$ on $\mathbb{S}^2$. As an alternative, the surfaces $\partial\mathscr{B}_1$ and $\partial\mathscr{B}_2^*$ can be sampled directly. In the method adopted for sampling spherocones, the surface of each body is divided into four parts: the spherical cap, the truncated cone on the side, the disk at the base, and the toroidal surface joining the latter two. Each of these parts is sampled via a specific function, with probability equal to the ratio between their area and that of the entire surface. Sampling of spherodisks and spherorods is performed in a similar way.

Direct sampling is then used for generating random points from the target surface through the equation

$$\boldsymbol{r}_{12}(\boldsymbol{v}_p) = p + \boldsymbol{r}_2^*(\boldsymbol{v}_p), \tag{B2}$$

where p is a random point on $\partial\mathscr{B}_1$ and $\boldsymbol{v}_p$ is the unit outer normal at p. (B2) alone is not sufficient, however, since any area of positive measure on $\partial\mathscr{B}_2^*$ where K is 0 generates a "hole" in the sampling of $\partial\mathscr{B}_e\{\mathscr{B}_1,\mathscr{B}_2\}$; this effect is described in Fig. 17 and exemplified by the point cloud shown in Fig. 18(a). For this reason, a second method, dual to the one based on (B2), supplements it: in this, a random point p on $\partial\mathscr{B}_2^*$ is translated by the radial mapping of $\mathscr{B}_1$ evaluated at $\boldsymbol{v}_p$. The two methods are applied with equal probability.

Even the combination of both these methods, however, may leave some areas of $\partial\mathscr{B}_e\{\mathscr{B}_1,\mathscr{B}_2\}$ unsampled, as shown in Fig. 18(b). The problem arises with any two line segments on $\partial\mathscr{B}_1$ and $\partial\mathscr{B}_2^*$, respectively, over which K is positive and the surface normal is the same, but the two segments fail to be parallel: each has zero probability of being sampled via either (B2) or its dual, yet their Minkowski addition is a flat region of positive measure on $\partial\mathscr{B}_e$. For the class of bodies considered here, the presence of such segments can be determined analytically and a specific sampling function can be added. For instance, in the case of two spherocones, there are two pairs of such segments, belonging to the truncated cone on the lateral surface of each body. From direct computation, a first pair of segments is characterized by the angles

$$\vartheta_1 = \arctan(\gamma_1,\lambda_1), \quad \vartheta_2 = \arctan(-\gamma_2,-\lambda_2), \tag{B3}$$

while a second pair is characterized by

$$\vartheta_1 = \arctan(-\gamma_1,\lambda_1), \quad \vartheta_2 = \arctan(\gamma_2,-\lambda_2). \tag{B4}$$

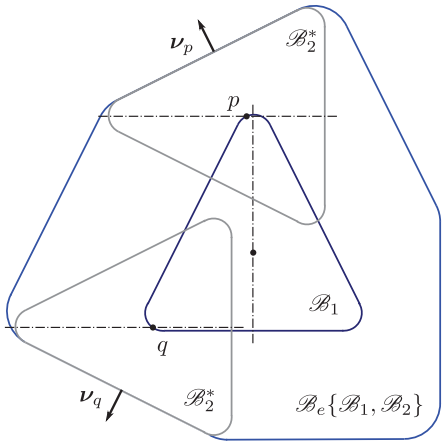

FIG. 17. (Color online) Cross section of the excluded body $\mathscr{B}_e\{\mathscr{B}_1,\mathscr{B}_2\}$ of bodies $\mathscr{B}_1$ and $\mathscr{B}_2$, both congruent to a spherocone $\mathscr{C}_r^\alpha$ with $\alpha = \arctan(1/2) \doteq 26.6^\circ$ and $r = L/10$, and having axes at the angle $\theta = 90^\circ$. The dash-dotted lines represent the axes of symmetry of $\mathscr{B}_1$ and of $\mathscr{B}_2^*$ in the configurations where the centroid c_2 of $\mathscr{B}_2^*$ is either in p or in q. When $\partial\mathscr{B}_1$ is sampled first and then the translation $\boldsymbol{r}_2^*(\boldsymbol{v})$ is added, some parts of $\partial\mathscr{B}_e\{\mathscr{B}_1,\mathscr{B}_2\}$ remain unsampled. For instance, the two subsets having normal $\boldsymbol{v}_p$ and $\boldsymbol{v}_q$, respectively, have zero probability of being sampled.

In these equations, ϑ_1 and ϑ_2 are azimuth angles in the cylindrical frames around the axes of $\mathscr{B}_1$ and $\mathscr{B}_2$, respectively. The two angles are measured with respect to the plane containing both axes. Furthermore,

$$\gamma_1 := \frac{\sqrt{-2\cos\theta\sin\alpha_1\sin\alpha_2 + \cos^2\alpha_1 - \sin^2\alpha_1 - \cos^2\theta}}{\cos\alpha_1\sin\theta},$$

$$\gamma_2 := \frac{\sqrt{-2\cos\theta\sin\alpha_1\sin\alpha_2 + \cos^2\alpha_1 - \sin^2\alpha_1 - \cos^2\theta}}{\cos\alpha_2\sin\theta},$$

$$\lambda_1 := \frac{\cos\theta\sin\alpha_1 + \sin\alpha_2}{\cos\alpha_1\sin\theta},$$

$$\lambda_2 := \frac{\cos\theta\sin\alpha_2 + \sin\alpha_1}{\cos\alpha_2\sin\theta},$$

where θ is the angle between the two axes and α_1 and α_2 are the semiamplitudes of $\mathscr{B}_1$ and $\mathscr{B}_2$, respectively. Note that, when

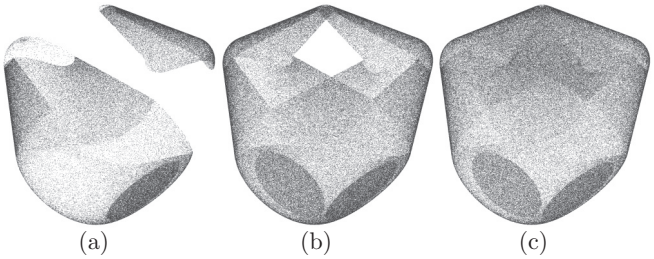

FIG. 18. Three "clouds" of random points from the same surface $\partial\mathscr{B}_e\{\mathscr{B}_1,\mathscr{B}_2\}$ as in Fig. 17. In (a), only the sampling procedure (B2) is applied: the presence of unsampled regions is apparent. In (b) both (B2) and its dual procedure are applied; there are still two holes corresponding each to a pair of segments on $\partial\mathscr{B}_1$ and $\partial\mathscr{B}_2^*$ that have parallel tangent planes. The cloud in (c) is produced by adding a specific function for these pairs of segments: it covers $\partial\mathscr{B}_e\{\mathscr{B}_1,\mathscr{B}_2\}$ entirely.

θ is 0°, the segments in each pair are parallel and the holes vanish.

With the addition of a specific sampling function based on (B3) and (B4), the procedure can effectively generate a stream of random points that provide complete coverage of $\partial\mathscr{B}_e$ for any pair of bodies in the class considered, even when the two have different parameters.

2. Surface triangulation

The procedure adopted to triangulate the target surface is based on the SOAM algorithm [54], which combines one method, based on the NEURAL GAS algorithm [55], for positioning a set of vertices in three-dimensional space through the stochastic optimization of a functional (in this case the average squared distance between random points from $\partial\mathscr{B}_e$ and their closest vertex) with another method for the incremental construction of the so-called *witness complex* [56], i.e., a particular simplicial complex that, under specific conditions, coincides with the *restricted Delaunay complex* induced by $\partial\mathscr{B}_e$ over the set of vertices. It can be shown that this complex, when it achieves the form of a closed triangulation, is isotopic to $\partial\mathscr{B}_e$ and the Hausdorff distance to the latter is $O(\varepsilon^2)$, where ε is the Hausdorff distance between $\partial\mathscr{B}_e$ and the set of its vertices.

The SOAM algorithm is also a *growing* self-organizing network, in the sense that it automatically creates as many vertices as are required for the reconstruction of the target surface. More precisely, in the resulting triangulation, the length of each edge must lie within a range of values that can be predefined as an input parameter to the algorithm. Indirectly, this also defines an upper bound for the Hausdorff distance ε, and hence for the approximation error to the target surface.

Given that the density of the triangulation obtained, as defined by the range of the lengths of its edges, does *not* depend on the sampling probability over the target surface—complete coverage apart, the procedure does not require uniform sampling and, in particular, it is robust with respect to oversampling. In addition, the construction of the triangulation occurs incrementally and in the same pipeline with the sampling procedure, i.e., one random point at a time

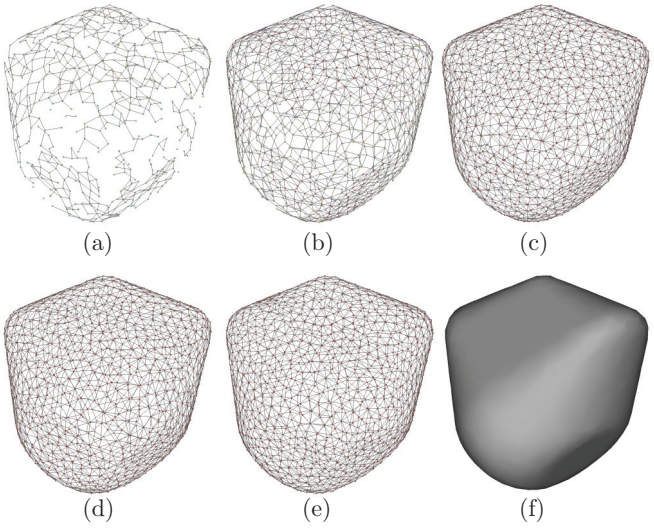

FIG. 19. The reconstruction process during which SOAM grows and adapts a set of vertices to a stream of random points from the surface $\partial\mathscr{B}_e$ in Fig. 17. A simplicial complex is also built progressively, until a complete triangulation is achieved and the procedure terminates. In the case shown here, the complete triangulation contains 1157 vertices and 2310 faces.

Therefore, the overall algorithm terminates automatically as soon as the point cloud is dense enough and the triangulation is complete. Clearly, such a completion can occur a different speeds: for instance, in Fig. 19, the reconstruction process takes longer in the lower parts of the surface, where the sampling probability is lower (see also Fig. 18).

The main advantage of using the SOAM algorithm in this context is its capability of self-detecting when the reconstruction process is complete, which reduces the time required for extensive, repeated runs like the ones needed for computing the isotropic averages shown in Fig. 8. To obtain the results presented here, an implementation written in Java was run on a computer with an Intel Core2 Quad Q6600 2.40 GHz processor, with 4 Gbytes of RAM. Each of the 561 reconstructions was completed on average in 182 s.

[1] D. Frenkel, in Proceedings of the 20th IUPAP International Conference on Statistical Physics [Physica A **263**, 26 (1999)].
[2] L. Onsager, Ann. N. Y. Acad. Sci. **51**, 627 (1949), reprinted in [3], pp. 625–657.
[3] T. J. Sluckin, D. A. Dunmur, and H. Stegemeyer, *Crystals that Flow* (Taylor & Francis, London, 2004).
[4] A. Haji-Akbari, M. Engel, A. S. Keys, X. Zheng, R. G. Petschek, P. Palffy-Muhoray, and S. C. Glotzer, Nature (London) **462**, 773 (2009).
[5] A. Haji-Akbari, M. Engel, and S. C. Glotzer, Phys. Rev. Lett. **107**, 215702 (2011).
[6] P. F. Damasceno, M. Engel, and S. C. Glotzer, Science **337**, 453 (2012).
[7] S. C. Glotzer, Nature (London) **481**, 450 (2012).
[8] J. P. Doye and W. C. Poon, Curr. Opin. Colloid Interface Sci. **11**, 40 (2006).
[9] W. Liu, D. Bratko, J. M. Prausnitz, and H. W. Blanch, Biophys. Chem. **107**, 289 (2004).
[10] B. H. Zimm, J. Chem. Phys. **14**, 164 (1946).
[11] B. Neal, D. Asthagiri, and A. Lenhoff, Biophys. J. **75**, 2469 (1998).
[12] A. George and W. W. Wilson, Acta Crystallogr., Sect. D: Biol. Crystallogr. **50**, 361 (1994).
[13] A. George, Y. Chiang, B. Guo, A. Arabshahi, Z. Cai, and W. Wilson, in *Macromolecular Crystallography Part A*, Methods in Enzymology, Vol. 276, edited by J. Charles W. Carter, (Academic Press, Waltham, Massachusetts, 1997), pp. 100–110.
[14] A. C. Dumetz, A. M. Chockla, E. W. Kaler, and A. M. Lenhoff, Biochim. Biophys. Acta, Proteins Proteomics **1784**, 600 (2008).

[15] M. A. Blanco, E. Sahin, Y. Li, and C. J. Roberts, J. Chem. Phys. **134**, 225103 (2011).
[16] E. Sahin, A. O. Grillo, M. D. Perkins, and C. J. Roberts, J. Pharm. Sci. **99**, 4830 (2010).
[17] N. Kern and D. Frenkel, J. Chem. Phys. **118**, 9882 (2003).
[18] Y. Li, B. A. Ogunnaike, and C. J. Roberts, J. Pharm. Sci. **99**, 4543 (2010).
[19] H. Minkowski, Math. Ann. **57**, 447 (1903).
[20] B. M. Mulder, Mol. Phys. **103**, 1411 (2005).
[21] A. M. Sonnet and E. G. Virga, Phys. Rev. E **77**, 031704 (2008).
[22] F. Bisi, A. M. Sonnet, and E. G. Virga, Phys. Rev. E **82**, 041709 (2010).
[23] J. P. Straley, Phys. Rev. A **10**, 1881 (1974).
[24] M. Piastra and E. G. Virga, Soft Matter **8**, 10969 (2012).
[25] A. J. Stone, *The Theory of Intermolecular Forces*, 2nd ed. (Oxford University Press, Oxford, 2013).
[26] C.-C. Wang, Arch. Rational Mech. Anal. **36**, 166 (1970).
[27] F. Bisi, R. Rosso, E. G. Virga, and G. E. Durand, Phys. Rev. E **78**, 011705 (2008).
[28] G. J. Vroege and H. N. W. Lekkerkerker, Rep. Prog. Phys. **55**, 1241 (1992).
[29] M. Piastra and E. G. Virga (unpublished).
[30] See Supplemental Material at http://link.aps.org/supplemental/10.1103/PhysRevE.88.032507, showing a gallery of views for the reconstructed shapes of the excluded body $\mathscr{B}_e$ of two congruent spherocones $\mathscr{C}_r^\alpha$ with $\alpha = \arctan(1/2) \doteq 26.6^\circ$ and $r = R/5$, which corresponds to $\varrho = r/L = 1/5\sqrt{5} \doteq 0.09$. The values α_0 of α at which the isotropic average $\langle v_e \rangle$ attains its minimum is $\alpha_0 \doteq 25.9^\circ$ and the relative minimum of the scaled excluded volume v_e occurs at $\theta_0 \doteq 59.5^\circ$.
[31] K. Große-Brauckmann, Experiment. Math. **6**, 33 (1997).
[32] L. J. Ellison, D. J. Michel, F. Barmes, and D. J. Cleaver, Phys. Rev. Lett. **97**, 237801 (2006).
[33] P. Palffy-Muhoray, E. G. Virga, and X. Zheng (unpublished).
[34] A. M. Sonnet and E. G. Virga, *Dissipative Ordered Fluids. Theories for Liquid Crystals* (Springer, New York, 2012).
[35] T. Bonnesen and W. Fenchel, in *Theory of Convex Bodies*, edited by L. Boron, C. Christenson, and B. Smith, with the collaboration of W. Fenchel (BCS Associates, Moscow, ID, 1987), translated from the German *Theorie der konvexen Körper* (Springer, Berlin, 1934).
[36] H. Hadwiger, *Altes und Neues über konvexen Körper* (Birkhäuser, Basel, 1955).
[37] R. Schneider, *Convex Bodies: The Brunn-Minkowski Theory*, Encyclopedia of Mathematics and its Applications Vol. 44 (Cambridge University Press, Cambridge, 1993).
[38] H. Brunn, Inaugural Dissertation, Über Ovale und Eiflächen, München, 1887.
[39] J.-M. Morvan, *Generalized Curvatures*, Geometry and Computing, Vol. 2 (Springer, Berlin, 2008).
[40] W. Blaschke, *Vorlesungen über Integralgeometrie*, 3rd ed. (Deutsch. Verlag Wiss., Berlin, 1955).
[41] M. E. Gurtin, E. Fried, and L. Anand, *The Mechanics and Thermodynamics of Continua* (Cambridge University Press, Cambridge, 2010).
[42] H. L. Royden, *Real Analysis*, 2nd ed. (Macmillan, New York, 1968).
[43] H. Minkowski, *Geometrie der Zahlen* (Teubner, Leipzig, 1910).
[44] J. Favard, Bull. Soc. Math. France **61**, 63 (1933).
[45] L. A. Santaló, *Integral Geometry and Geometric Probability*, 2nd ed. (Cambridge University Press, Cambridge, 2004).
[46] H. Boerner, *Representations of Groups: with Special Consideration for the Needs of Modern Physics* (North-Holland, Amsterdam, 1963).
[47] D. Vvedensky, Group Theory, http://www.cmth.ph.ic.ac.uk/people/d.vvedensky/courses.html.
[48] G. S. Singh and B. Kumar, Ann. Phys. (NY) **294**, 24 (2001).
[49] T. Kihara, Rev. Mod. Phys. **25**, 831 (1953).
[50] T. Kihara, J. Phys. Soc. Jpn. **8**, 686 (1953).
[51] A. Isihara, J. Chem. Phys. **18**, 1446 (1950).
[52] A. Isihara and T. Hayashida, J. Phys. Soc. Jpn. **6**, 40 (1951).
[53] A. Isihara and T. Hayashida, J. Phys. Soc. Jpn. **6**, 46 (1951).
[54] M. Piastra, Neural Networks **41**, 96 (2013).
[55] T. Martinetz, S. Berkovich, and K. Schulten, IEEE Trans. Neural Networks **4**, 558 (1993).
[56] L. J. Guibas and S. Y. Oudot, Discrete Comput. Geom. **40**, 325 (2008).